PROCEEDINGS OF SCIENCE

Highlights from the Pierre Auger Observatory

E. Santos*,
Institute of Physics (FZU) of the Czech Academy of Sciences
Na Slovance 2, Prague, Czech Republic

for the Pierre Auger Collaboration
Observatorio Pierre Auger
Av. San Martín Norte 304, 5613 Malargüe, Argentina
Full author list: http://www.auger.org/archive/authors_2018_06.html
E-mail: auger_spokespersons@fnal.gov

The existence of a cosmic ray flux of a still unknown origin with particles reaching energies millions of times higher than those attained at the LHC continues to intrigue the scientific community. The Pierre Auger Observatory, the largest cosmic ray detector in the world, was built to study the cosmic rays with $E > 10^{17}$ eV with unprecedented statistics. Taking continuous data since 2004, the Pierre Auger Collaboration has published numerous results about the properties of Ultra-High Energy Cosmic Rays. Recently it has determined, with a $5.2\,\sigma$ significance, that the arrival directions of cosmic rays with energies above 8 EeV are anisotropic and can be described by a dipole whose direction favors an extragalactic origin of Ultra-High Energy Cosmic Rays. At an intermediate angular scale, the two largest departures from isotropy for the arrival directions of events with $E > 39$ EeV and $E > 60$ EeV are best described by a correlation with two nearby populations of extragalactic gamma-ray sources, namely starburst galaxies and AGNs. Photon and neutrino searches for events above 1 EeV and 0.1 EeV, respectively, resulted in no candidates so far, allowing Auger to put stringent limits to the flux of these particles. In the multi-messenger astronomy era, Auger is actively participating in neutrino searches in coincidence with gravitational wave events. Currently, the Observatory is undergoing a major upgrade which aims at an improved determination, event-by-event, of the nuclear mass composition of cosmic rays near the region of the flux suppression with increased statistics.

Frontier Research in Astrophysics - III (FRAPWS2018)
28 May - 2 June 2018
Mondello (Palermo), Italy

*Speaker.

PoS(FRAPWS2018)025

1. Introduction

The discovery of cosmic rays more than one century ago motivated innumerous experiments to determine the origin and nature of these particles. More than 80 years of cosmic ray experiments allowed to establish the existence of a particle flux of non-thermal origin which steeply falls by more than 30 orders of magnitude as the energy of cosmic rays extends by more than 10 orders of magnitude. The few features of the cosmic ray spectrum can provide valuable hints about their origin, acceleration, propagation mechanisms and composition, however, the exact explanations causing each spectral feature are still under discussion. It is assumed that cosmic rays with maximum energies up to several EeV could come from sources within the Galaxy, whereas the most energetic cosmic rays are believed to arrive from nearby extragalactic sources located in a sphere not bigger than $\sim 250\,\mathrm{Mpc}$ radius [1]. Yet, the region where the transition between these two populations takes place is still undetermined.

At energies around $10^{15}\,\mathrm{eV}$, cosmic rays can only be detected indirectly through the large numbers of secondary particles which are produced from their interaction in the Earth's atmosphere using either arrays of particle detectors at the ground or fluorescence telescopes. Above $10^{19}\,\mathrm{eV}$, the steeply falling flux of cosmic rays reaches only about one particle per square kilometer per year demanding for areas of particle detectors of the order of $\sim 1000\,\mathrm{km}^2$, as it is the case of the Telescope Array [2], in the Northern Hemisphere and the Pierre Auger Observatory in the Southern Hemisphere [3]. In this case, the reconstruction of the cosmic ray properties suffers from large systematic uncertainties as they must rely on the predictions of Monte Carlo simulations of Extensive Air Showers (EAS) using high energy hadronic interactions models which often need to be extrapolated to $\sqrt{s} \sim 100\,\mathrm{TeV}$, one order of magnitude above the nominal energy at the LHC.

In this manuscript are presented the most recent results of the Pierre Auger Observatory regarding the confirmation of the extragalactic origin of the highest energy cosmic rays and a possible correlation of their sources with nearby populations of starburst galaxies and AGNs. The results of the searches for neutral particle messengers and multi-messenger studies are reviewed as well. The Pierre Auger Observatory is described in Section 2, a discussion about the most recent results of the Observatory is presented in Section 3. Finally, the ongoing upgrade of the Pierre Auger Observatory, the AugerPrime is introduced in Section 4.

2. Pierre Auger Observatory

The Pierre Auger Observatory, located near the city of Malargüe in the Argentinian province of Mendoza at $\sim 1400\,\mathrm{m}$ a. s. l. (corresponding to an average vertical atmospheric depth of $X_{\mathrm{ground}} = 880\,\mathrm{g\,cm^{-2}}$), is the largest cosmic ray detector in the world. It uses a hybrid technique which combines a Surface Detector Array (SD) and a Fluorescence Detector (FD) to study the most energetic cosmic rays with unprecedented statistics.

The SD samples the lateral distribution of charged particles at the ground with $\sim 100\%$ duty cycle. It is composed of more than 1600 water-Cherenkov stations arranged in a triangular grid of 1500 m spacing covering an area of $3000\,\mathrm{km}^2$ and it is fully efficient to the detection of cosmic rays with energies above $10^{18.5}\,\mathrm{eV}$ ($10^{18.6}\,\mathrm{eV}$) for events with zenith angles $\theta < 60^\circ$ ($62^\circ < \theta < 80^\circ$).

The energy range of the SD was lowered to 3×10^{17} eV by the inclusion of extra 60 stations in a 750 m triangular grid, comprising $\sim 23.5\,\mathrm{km}^2$ of the whole array.

The FD detects the ultraviolet light emitted by the excited nitrogen molecules in the atmosphere, providing an almost calorimetric estimation of the energy of the shower, and also a direct measurement of the depth of the shower maximum, X_{max}. The FD comprises 24 fluorescence telescopes housed in four buildings at the array periphery which observe the atmosphere above the SD in clear and moonless nights, reaching a duty cycle of $\sim 15\%$. The low energy extension of the FD is called HEAT (High Elevation Auger Telescopes), and it is composed of three additional fluorescence telescopes at the Coihueco site. The HEAT telescopes can work both in the downward and upward mode, encompassing a total field of view (FoV) from 2° to 60° in elevation. When working in the upward mode, the HEAT telescopes observe the FoV region from 30° to 60°, complementary to the common FoV range of the standard FD telescopes, enabling the detection of nearby showers with energies ranging from $10^{17.2}$ eV to $10^{17.8}$ eV. The events detected both by the FD and the SD are called hybrid. A complete description of the Observatory and its instrumentation can be found in [3]. The layout of the Observatory is shown in Figure 1.

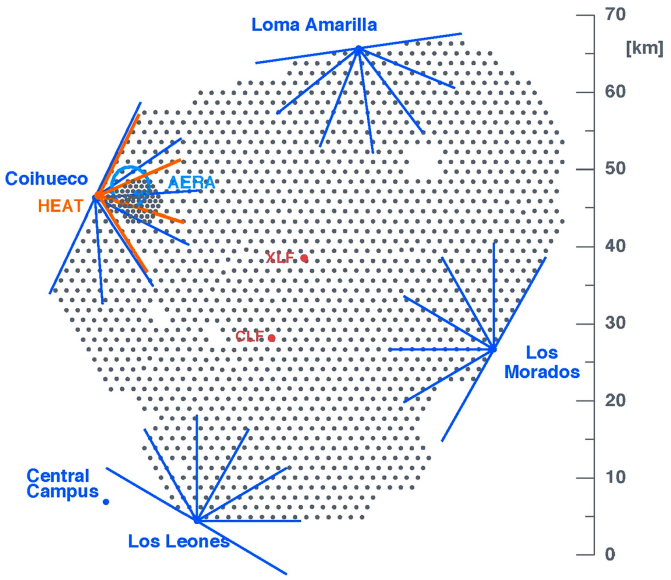

Figure 1: Schematic sketch of the Pierre Auger Observatory.

3. Results

Below are summarized some of the most recent results of the Pierre Auger Observatory regarding studies of the nuclear mass composition of cosmic rays, the searches for large and intermediate scale anisotropies in the arrival directions of the most energetic cosmic rays. Finally, at the end of the section are presented some results about the photon and neutrino searches, and multi-messenger studies focusing on the follow-ups of the Pierre Auger Observatory on neutrino searches in coincidence with gravitational wave events.

3.1 Nuclear mass composition

The Fluorescence Detector (FD) of the Pierre Auger Observatory provides a direct measurement of the depth of the shower maximum, $X_{\rm max}$, one of the most robust variables for mass composition studies. Here are presented the results for the interpretation of the nuclear mass composition of cosmic rays detected by the fluorescence telescopes of the Pierre Auger Observatory with energies ranging from $10^{17.2}$ to about $10^{19.6}$ eV using the $\langle X_{\rm max}\rangle$ and $\sigma\,(X_{\rm max})$ moments. Additionally, the $X_{\rm max}$ distributions are also interpreted in terms of mass fractions of proton, Helium, Nitrogen and Iron primaries, as predicted by several post-LHC hadronic interactions models.

The data were divided into two independent data sets. One dataset contains events detected by the standard FD telescopes between 1 December 2004 and 31 December 2015 for showers with energies above $10^{17.8}$ eV. The second dataset uses events recorded both by the HEAT and Coihueco telescopes, HeCo, with energies ranging from $10^{17.2}$ to $10^{17.8}$ eV recorded between 1 June 2010 to 31 December 2015. All the events used in this analysis are hybrid, i.e., their geometries were reconstructed using information of the arrival times of the cameras of the FD telescopes and of the shower front at the ground measured by the SD station closest to the shower axis. The selected events were recorded in periods of stable running conditions and good atmospheric conditions as described in [4]. Additionally, fiducial FoV cuts are applied to reduce the detector effects on the $X_{\rm max}$ distributions, as described in [5, 4], so that each event has a resolution of the reconstructed $X_{\rm max}$ better than $40\,{\rm g\,cm^{-2}}$. After all cuts, a total of 16778 and 25688 events were used in the HeCo and standard FD datasets, respectively. The results for the $\langle X_{\rm max}\rangle$ and $\sigma\,(X_{\rm max})$ are shown in Figure 2, and the energy binning for the data is $\Delta\lg\,(E/{\rm eV}) = 0.1$.

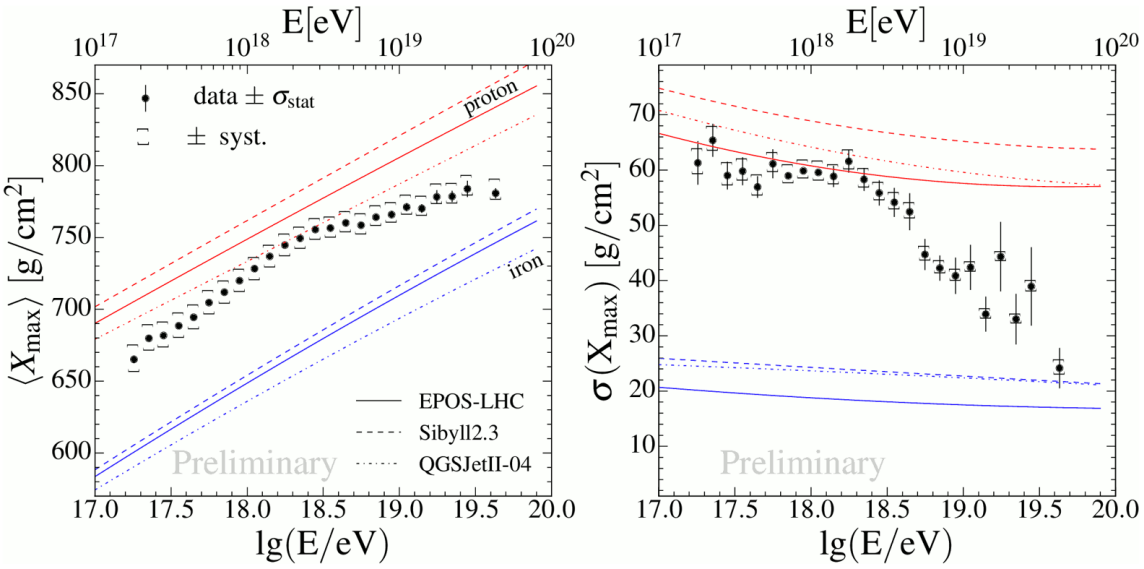

Figure 2: Mean (left) and standard deviation (right) of the $X_{\rm max}$ distributions as a function of energy. The full, dotted and dashed lines represent the predictions of hadronic interactions model for proton (red) and iron (blue) induced showers [5].

From the left panel of Figure 2, it can be seen that the elongation rate (the rate of change of $\langle X_{\rm max}\rangle$ as a function of energy) between $10^{17.2}$ and $10^{18.33}$ eV is $(79\pm1)\,{\rm g\,cm^{-2}\,decade^{-1}}$, larger

than the expected value for a constant mass composition ($\sim 60\,\mathrm{g\,cm^{-2}\,decade^{-1}}$), indicating that the nuclear mass composition is getting lighter with increasing energy. After $10^{18.33}$ eV, there is a break in the elongation rate, and it becomes $(26 \pm 2)\ \mathrm{g\,cm^{-2}\,decade^{-1}}$, meaning that the nuclear mass composition is getting heavier with increasing energy. In the right panel of Figure 2 is shown the variation of the $\sigma\,(X_{\mathrm{max}})$ with energy. Also here, the nuclear mass composition is compatible with a light component for energies below $10^{18.33}$ eV, and becoming heavier above that energy.

In another analysis, the distributions of X_{max} in each energy bin were compared to mixes of proton (p), Helium (He), Nitrogen (N) and Iron (Fe) primaries as obtained from CONEX [6] simulations using the post-LHC models EPOS-LHC [7], QGSJetII-04 [8], and Sybill 2.3 [9]. The model distributions were parameterised by a Gaussian convoluted with an exponential function as described in [10]. The results of the fitted mass fractions are presented in Figure 3.

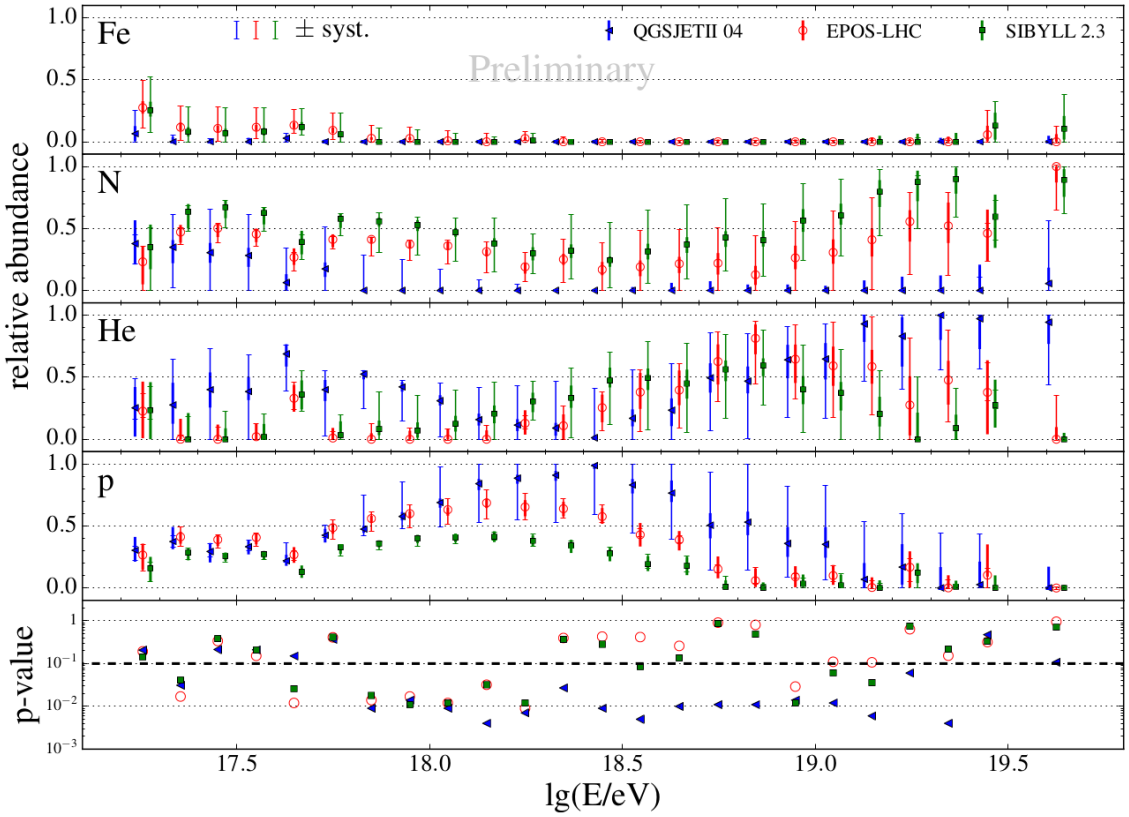

Figure 3: Mass fraction fits obtained using parameterizations of the expected X_{max} distributions using the Auger data collected with the FD. The error bars indicate the statistical (smaller cap) and the systematic uncertainties (larger cap). The bottom panel indicates the $p-$values for the goodness of the fits [5].

From Figure 3, it can be seen that Fe seems to be almost absent over the whole energy range except possible small fractions at the lowest and highest energies. There is a high percentage of protons for energies below 10^{19} eV, followed by an increase of the He fraction arising at $\sim 10^{18.6}$ eV and dropping at $\sim 10^{19.2}$ eV, succeeded by an increase of the Nitrogen fraction at $\sim 10^{19.3}$ eV. However, one should note that the interpretation of the mass fractions is model dependent. The large number of $p-$values below the 0.1 dashed line indicates that the models were not able to find good combinations of fractions describing the measured X_{max} distributions.

Due to the limited duty cycle of the FD, there are very few events at the highest energies, making difficult further mass composition studies with this detector. However, it is possible to use the time structure of the signals recorded by the Surface Detector (SD), which has nearly 100% duty cycle. In [11, 12], the $X_{\rm max}$ of the shower was inferred from the risetime, $t_{1/2}$, of the time traces of the SD, allowing to infer the mass composition of showers for energies ranging from 0.3 to more than 100 EeV. The risetime $t_{1/2}$ is defined as the time taken by the total signal to go from 10% to 50% and it depends of the distance to the shower axis, zenith angle, and energy of the shower. For the method to be used, the risetimes of the several stations of each event, in a narrow energy region, are related to a function which describes the measured risetimes, called the *benchmark*. In a posterior step, the risetimes of the stations in a particular event are compared to the relevant times from the benchmark function, where the time difference between the measured risetime at a given station and the one given by the function is called Δ_i. Finally, each shower is characterized for the average values of Δ_i, which correlate with the depth of the shower maximum $X_{\rm max}$. The results of the $X_{\rm max}$ determined from the Δ method (blue circles and red squares), and $X_{\rm max}$ (open squares) direct measurements are displayed in Figure 4. Both measurements agree well with each other. The SD data allow to gain two extra energy bins at the highest energies, with $\langle X_{\rm max}\rangle$ suggesting, at a 3σ significance, that the nuclear mass does not continue to grow with energy.

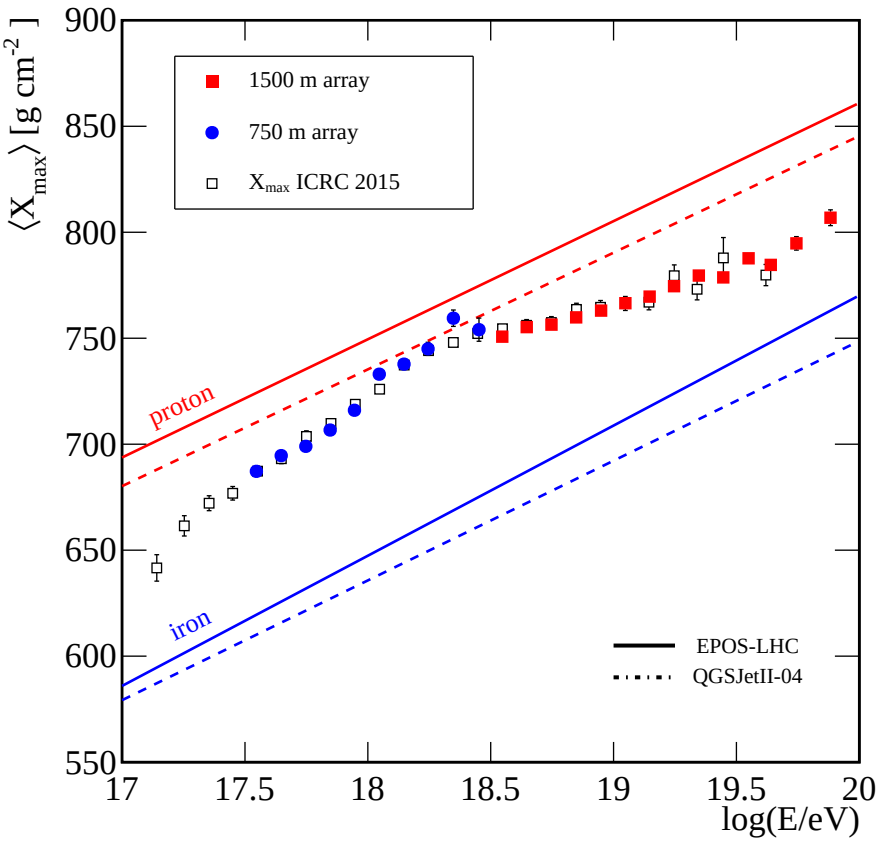

Figure 4: Comparison of $\langle X_{\rm max}\rangle$ obtained using the Δ method (blue circles and red squares), and the $\langle X_{\rm max}\rangle$ obtained from the FD (open squares). The error bars are only statistical [12].

3.2 Anisotropies

The nearly 100% duty cycle and the 1.2 m depth of the water-Cherenkov stations of the SD allow the Pierre Auger Observatory to observe 85% of the whole sky with a nearly uniform exposure in right ascension.

In this subsection are presented the latest results on the large and intermediate angular scale anisotropies of the arrival directions of cosmic rays with zenith angles with $\theta < 80^\circ$, corresponding the declination range $-90^\circ < \delta < 45^\circ$.

The arrival directions of cosmic rays are determined through the relative arrival times of the shower front at each of the triggered stations, where the angular resolution for the energies of interest in these studies is better than 1° [3]. Due to the geomagnetic field, the shower reconstruction using the SD differs for showers with zenith angles below and above 60° [13, 14]. Also for showers with $\theta < 60^\circ$, the atmospheric effects produce systematic modulations in the rate which have to be corrected [15]. The details of the shower reconstruction using the SD for events with $\theta < 60^\circ$ can be found in [16], while the reconstruction of events with $\theta > 60^\circ$ is described in [13]. In both zenith regions the energy estimators were calibrated using hybrid events. The statistical uncertainty in the energy determination is $< 16\%$ for events with $E > 4\,\mathrm{EeV}$ and $< 12\%$ for events with $E > 10\,\mathrm{EeV}$. The systematic uncertainty on the absolute energy scale is 14% over the whole energy and zenith angle ranges [17].

Large-scale anisotropy in the arrival direction of cosmic rays above 8 EeV This analysis was applied to data recorded by the SD between 1 January 2004 and 31 August 2016 for events with $E > 4\,\mathrm{EeV}$, the energy at which the array becomes fully efficient for showers with $62^\circ \leq \theta < 80^\circ$ [13], corresponding to a total exposure of $76800\,\mathrm{km^2}$ sr yr. Using the same procedure as in previous analyses [18, 19, 20], the data were divided into two energy bins, namely; $4\,\mathrm{EeV} < E < 8\,\mathrm{EeV}$, and $E \geq 8\,\mathrm{EeV}$. For the event to be selected, the station with the highest signal must be surrounded by five active stations, resulting in the selection of 113888 events, from which 81701 belong to the energy bin $4\,\mathrm{EeV} < E < 8\,\mathrm{EeV}$ and the remaining 32187 events have $E \geq 8\,\mathrm{EeV}$ [21, 22]. The study of large-scale anisotropy was performed by using a harmonic analysis in right ascension, α, where the first harmonic components a_α and b_α are given by:

$$a_\alpha = \frac{2}{\mathcal{N}} \sum_{i=1}^{N} \omega_i \cos\alpha_i \ , \ b_\alpha = \frac{2}{\mathcal{N}} \sum_{i=1}^{N} \omega_i \sin\alpha_i .$$

The sum runs over all the N detected events, each one with right ascension α_i, and $\mathcal{N} = \sum_{i=1}^{N} \omega_i$ is the normalization factor. The weights ω_i are introduced to take into account the non-uniformities in the array in right ascension, and for a tilt of the array toward the southeast introducing a harmonic dependence in azimuth of amplitude $0.3\% \tan\theta$ to the exposure. The amplitude r_α and the phase ϕ_α of the first harmonic of the modulation are calculated as:

$$r_\alpha = \sqrt{a_\alpha^2 + b_\alpha^2} \ , \ \tan\phi_\alpha = \frac{b_\alpha}{a_\alpha} .$$

The results for the amplitude, phase and the probability that the observed amplitudes are larger than the ones which could arise by chance due to fluctuations from an isotropic distribution for the two energy bins are shown in Table 1.

Table 1: Results for the amplitude r_α, phase ϕ_α and probability P of the observed amplitudes to arise by chance from an isotropic distribution.

Energy EeV	Amplitude r_α	Phase $\phi_\alpha\,(^\circ)$	Probability $P(\geq r_\alpha)$
4 to 8	$0.005^{+0.006}_{-0.002}$	80 ± 60	0.60
≥ 8	$0.047^{+0.008}_{-0.007}$	100 ± 10	2.6×10^{-8}

From [23], the probabilities in the rightmost column of Table 1 were calculated as:

$$P(r_\alpha) = \exp\left(-\mathcal{N} r_\alpha^2/4\right).$$

For the energy bin $4\,\mathrm{EeV} < E < 8\,\mathrm{EeV}$, the amplitude of the dipole is $r_\alpha = 0.005^{+0.006}_{-0.002}$, which has a probability of arising by chance from an isotropic distribution of $P(\geq r_\alpha) = 0.60$. However, for the events in $E \geq 8\,\mathrm{EeV}$, the amplitude of the first harmonic, which is $0.047^{+0.008}_{-0.007}$, has a probability of arising by chance from an isotropic distribution of only $P(\geq r_\alpha) = 2.6 \times 10^{-8}$, equivalent to a two-sided Gaussian significance of 5.6σ. The presence of this dipole, whose signal significance was found to grow with time, was already known. Penalizing for the previous analyses and by further studies where four additional lower-energy bins were examined gives a significance to the observed dipole of 5.2σ. The maximum modulation is at right ascension $100^\circ \pm 10^\circ$. In Figure 5 is shown the distribution of the normalized rate of events for $E \geq 8\,\mathrm{EeV}$ as a function of right ascension, along with the fit to a sinusoidal function corresponding to the first harmonic.

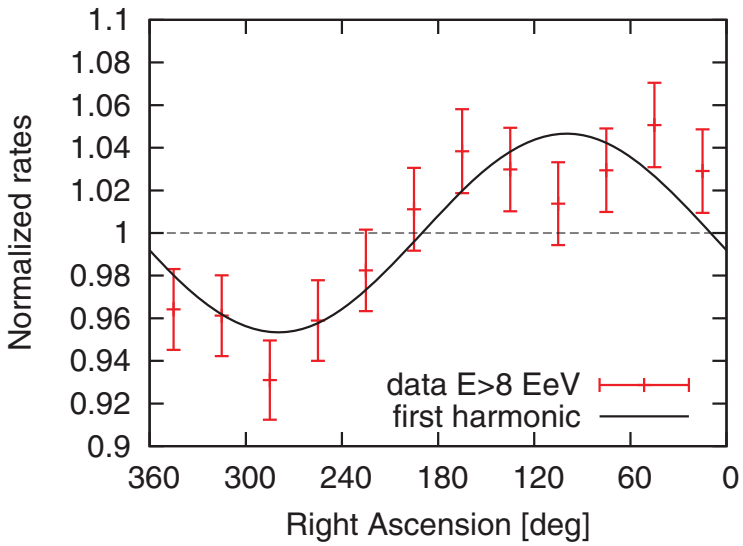

Figure 5: Normalized rate of events as a function of right ascension for $E \geq 8\,\mathrm{EeV}$. The error bars represent 1σ uncertainties [22].

To confirm the dipolar modulation, a sinusoidal and a constant function were fitted to the data shown in Figure 5. A $\chi^2/n = 10.5/10$ was obtained for the sinusoidal function, while a worse value of $\chi^2/n = 45/12$ resulted from the fit to a straight line.

The distribution of events with $E \geq 8\,\mathrm{EeV}$, in equatorial coordinates, is shown in Figure 6. The same is shown in Figure 7, but for galactic coordinates.

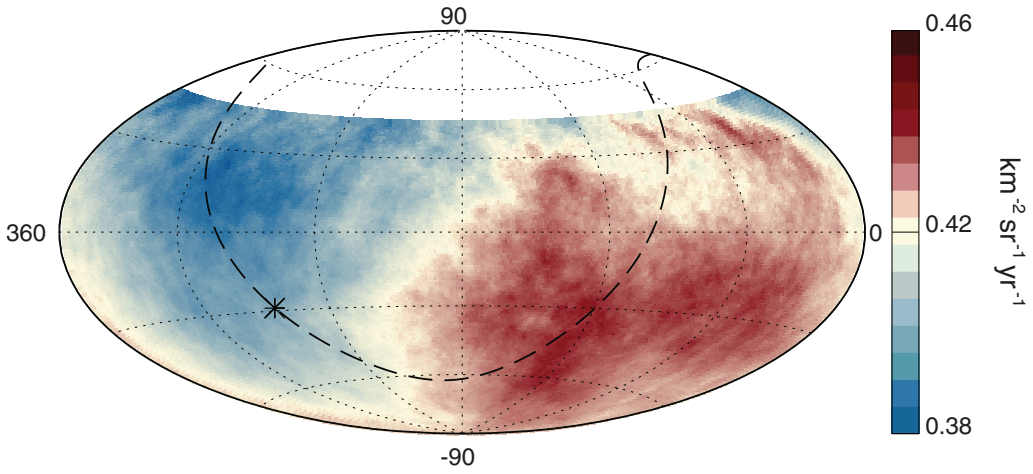

Figure 6: Sky map in equatorial coordinates of the cosmic ray flux for $E \geq 8\,\mathrm{EeV}$. For better visualization of the large-scale features, the arrivals directions of the events were smoothed with a 45° top-hat function [22]. The Galactic plane is represented by the dashed line and center is marked by an asterisk.

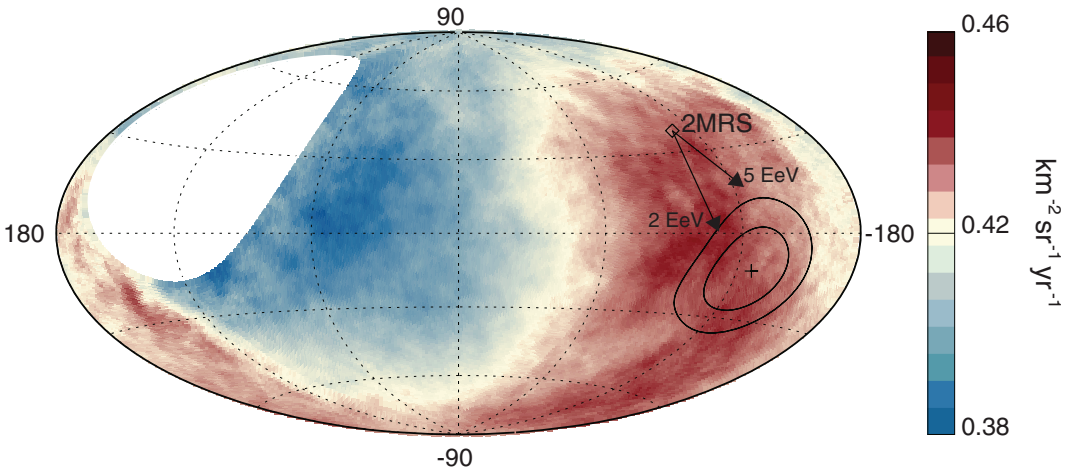

Figure 7: Sky map in galactic coordinates of the cosmic ray flux for $E \geq 8\,\mathrm{EeV}$ smoothed with a 45° top-hat function. The cross indicates the dipole direction and the contours mark the 68% and 95% confidence level regions [22]. The diamond marks the dipole direction of the 2MRS galaxy distribution. The arrows show the deflections expected from the Janson and Farrar model described in [24] for particles with $E/Z = 5$ or 2 EeV.

For $E \geq 8\,\mathrm{EeV}$, the amplitude of the dipole is $d = 6.5^{+1.3}_{-0.9}\%$, pointing to the equatorial coordinates $(\alpha_d, \delta_d) = (100°, -24°)$. A dipole anisotropy in the arrival direction of cosmic rays is expected from the Compton-Getting effect [25], as a result of the proper motion of the Earth in the rest frame of cosmic ray sources, but this effect is expected to contribute only with the amplitude

of 0.6% [26], which is much smaller value than the observed one. The maximum of the dipole lies $\sim 125^\circ$ away from the Galactic center, and there is no excess of events coming from the Galactic center, which strongly support the hypothesis that the origin of these cosmic rays is extragalactic. At $4\,\mathrm{EeV} < E < 8\,\mathrm{EeV}$ the dipole points to the direction $(\alpha_d, \delta_d) = (80^\circ, -75^\circ)$, close to the South Galactic Pole. Although the amplitude of the dipole in this energy range is not significant, it also disfavors a Galactic origin. In galactic coordinates, the dipole at $E \geq 8\,\mathrm{EeV}$ points in the direction $(\ell, b) = (233^\circ, -13^\circ)$, about 55° away from the 2MRS dipole. It is expected that the galactic magnetic field change the trajectory of cosmic rays. The tips of the arrows in Figure 7 show the direction of the dipole of the Ultra-High Energy Cosmic Ray (UHECR) flux arriving at Earth from sources distributed according to the 2MRS dipolar structure. Assuming the propagation of cosmic rays in the Galactic magnetic field with common rigidity values of $E/Z = 5\,\mathrm{EeV}$ and $2\,\mathrm{EeV}$, it is expected that the amplitude of the dipole to lower from about 90% to 70% of the original value.

Correlation studies with the arrival directions of cosmic rays with $E > 20\,\mathrm{EeV}$ with nearby extragalactic gamma-ray sources In [27] it is claimed that the non-thermal flux of FRI radio galaxies and misaligned BL Lac objects measured by *Fermi*-LAT within the GZK horizon could explain the observed emissivity of cosmic rays, calculated to be $\sim 10^{45}$ erg Mpc^{-3} yr^{-1} for $E > 10^{18}$ eV [28]. Based on this hypothesis, the arrival directions of 5514 events with $E > 20\,\mathrm{EeV}$ recorded between 1 January 2004 to 30 April 2017 with $\theta < 80^\circ$ by the Pierre Auger Observatory were analyzed in relation to the position of nearby (within a sphere of 250 Mpc radius) gamma-AGNs and starburst galaxies from the *Fermi*-LAT source catalogs. The total exposure for the considered period of data taking is $89720\,\mathrm{km}^2$ sr yr [30, 29].

The list of AGNs was taken from the second catalog of hard *Fermi*-LAT sources, the 2FHL catalog [31], while the starburst galaxies were selected from a sample also surveyed by *Fermi*-LAT [32]. In total, the two extragalactic gamma-ray populations used for this study are composed of 17 blazars and radio-galaxies and 23 starburst galaxies whose flux density is larger than 0.3 Jy.

Based on the analysis of [33], the effect of the attenuation of UHECRs arriving from each source was taken into account by using data-driven scenarios which reproduce the mass composition and spectral constraints of the data collected by the Pierre Auger Observatory. Given their proximity to the Earth, the effect of attenuation from starburst galaxies is less important than the one for AGN sources, resulting that $\sim 90\%$ of the accumulated flux from starburst galaxies emerges from a ~ 10 Mpc radius, while a ~ 150 Mpc radius was found for AGNs.

The sky model of UHECR was derived from the convolution of an isotropic component plus an anisotropic component due to the sources. The source contributions were modeled by a Fisher distribution centered on the source coordinates, the integral was set by its flux attenuated above an energy threshold and an angular width. The sky model has two free parameters which serve to maximize the correlation with the arrival directions of the measured cosmic rays, namely, the fraction of all events due to the sources, and the rms angular separation between an event and the search radius of the source in the anisotropic fraction. The maximum correlation was found using an unbinned maximum-likelihood, where the likelihood is the product over the UHECR events in the model density in the UHECR directions. The test statistics (TS) for deviation from isotropy is the likelihood ratio test between two hypothesis: the sky model of UHECR and the isotropic distribution of UHECR, being this last one the null hypothesis. The TS is maximized as a function

of the search radius and the anisotropic fraction. The analysis is then repeated for several energy thresholds. The results of the energy scan of the TS are presented in Figure 8, from which two maxima are observed.

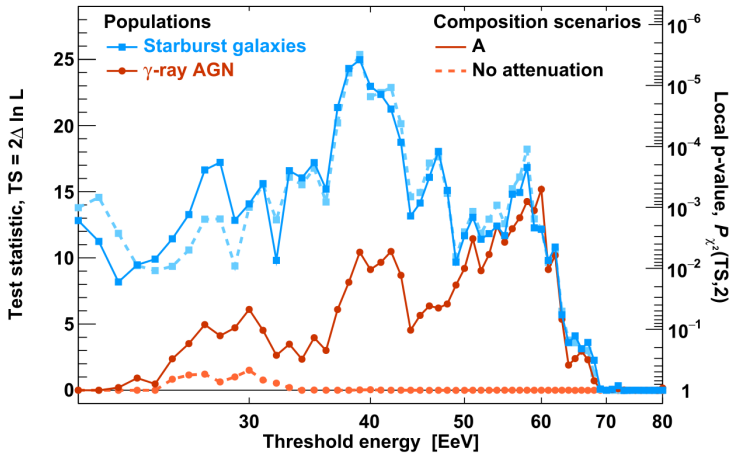

Figure 8: Test statistics scan over the threshold energy for starburst galaxies (blue) and AGNs (red) considering the cases with (full line) and without (dashed line) attenuation from the sources [30].

The maximum for starburst galaxies is observed for $E > 39$ EeV (894 events), with or without attenuation, whereas the maximum for AGNs is found for energies above 60 EeV (177 events), after taking into account the attenuation. Shifting the energy scale within the systematics of $\pm 14\%$[17], affects the maximum TS by ± 1 unit for AGNs and ± 0.3 for starburst galaxies. Penalizing for the energy scan, the maximum TS obtained for starburst galaxies and AGNs gives a 4.0σ and 2.7σ deviation from isotropy, respectively. The maximum deviation for starburst galaxies is found at an intermediate angular scale of $13^{+4}_{-3}{}^{\circ}$, and an anisotropic fraction of $10 \pm 4\%$. For AGNs, the maximum deviation is found at an angular scale of $7^{+4}_{-2}{}^{\circ}$, and an anisotropic fraction of $7 \pm 4\%$. In Figure 9 are shown the observed anisotropy maps for the populations of starburst galaxies ($E > 39$ EeV), and AGNs ($E > 60$ EeV).

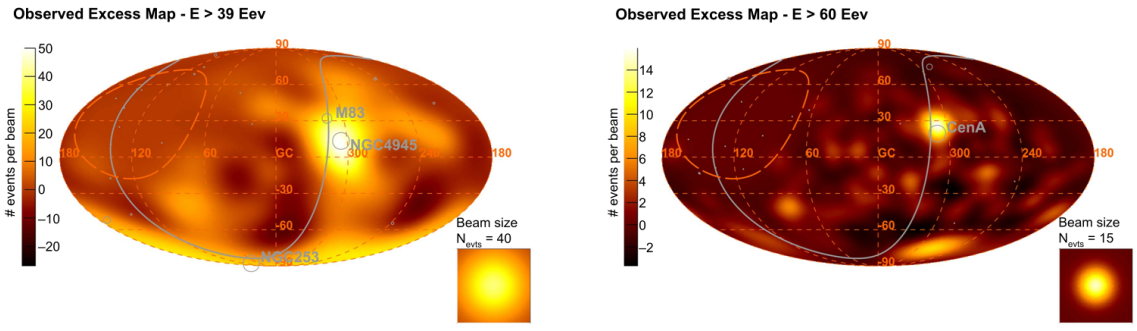

Figure 9: Observed excess map for starburst galaxies (left), and AGNs (right) [30].

A hot-spot is visible in the region of Centaurus A/M83/NGC 4945 group for both populations. The AGN model is dominated by the Centaurus A, which is 7°, and 13° away from the two starburst galaxies NGC 4945 and M83, respectively. For the starburst model it is also visible an excess near

the South Galactic Pole, interpreted as contributions from the galaxies NGC 1068 and NGC 253, which increase the anisotropy signal from $\sim 3\sigma$ to 4σ.

For events above 39 EeV, it was found that the contribution of a single population of AGNs is disfavored by 3.7σ relative to a combined model with 9% contribution from starburst galaxies and 1% contribution from AGNs, whereas for events with $E > 60$ EeV, the significance of considering a single AGN population or a combined contribution is nearly the same.

3.3 Neutral messengers

As it was shown in the results presented above, the charged nature of cosmic rays does not yet allow the identification of their sources. However, several astrophysical models describing the acceleration and propagation mechanisms of UHECR, such as the GZK-like processes [34, 35] also predict the existence of fluxes of Ultra-High Energy (UHE) photons and neutrinos whose detection would finally allow to answer this question [36, 37].

Below are presented the most recent results regarding the searches of a diffusive flux [38, 39, 40, 41], and point sources [42, 43, 44] of photons and neutrinos. Up to the present moment, no neutral candidates were found in the data, which allows the Pierre Auger Collaboration to put competitive limits to the fluxes of these particles.

Photons Photon induced showers have a much lower muonic content, a smaller footprint on the ground, and a deeper $\langle X_{\rm max}\rangle$, when compared to hadronic showers. For $E > 10$ EeV, the Landau-Pomeranchuk-Migdal (LPM) effect becomes important, and in this case, a superposition of cascades initiated by low energy photons would produce smaller values of $\langle X_{\rm max}\rangle$, and larger muonic to electromagnetic content when compared to "normal" photon induced showers at the same energy [45]. The searches for photon candidates use methods which compare the characteristics of hadronic showers and photon induced showers. Detailed procedures for photon searches using pure SD data can be found in [38], while searches for hybrid data are described in [42, 39, 43, 46]. The SD searches can be applied for events with $E > 10$ EeV and $30^\circ < \theta < 60^\circ$, whereas the searches with hybrid events are performed for $E > 1$ EeV and $\theta < 60^\circ$. In Figure 10 are shown the upper limits to the integrated photon flux as a function of energy. These limits put strong constraints on the current top-down models proposed to explain the origin of UHECR. Currently, the sensitivity of the hybrid photon searches, represented by the blue arrows in Figure 10, allows to test photon fractions of 0.1%, entering the photon flux regions proposed by some GZK scenarios.

The presence of a photon source in the sky would manifest through the detection of a clustering of photon induced showers arriving from a particular position in the sky. In [43], hybrid events in the energy range of $10^{17.3}$ eV to $10^{18.5}$ eV are used to look for clusterings of events arriving from 12 candidate photon point sources located in the declination range $-85^\circ < \delta < 20^\circ$. The source targets include objects located in the Galactic center region, and also nearby extragalactic sources such as the Large Magellan Cloud and Centaurus A. The reason to search for nearby sources is justified by the attenuation length of UHE photons which ranges from 90 kpc at $10^{17.3}$ eV, to 900 kpc at $E = 10^{18.5}$ eV. For all the 12 sources considered in [43], the measured and expected number of events within an opening angle of 1° had a statistical significance less than 3σ, meaning that no excess of events was found. In Figure 11, the Auger limits to the photon flux as a function of energy for the Galactic center region are shown. The Auger searches for point sources in the

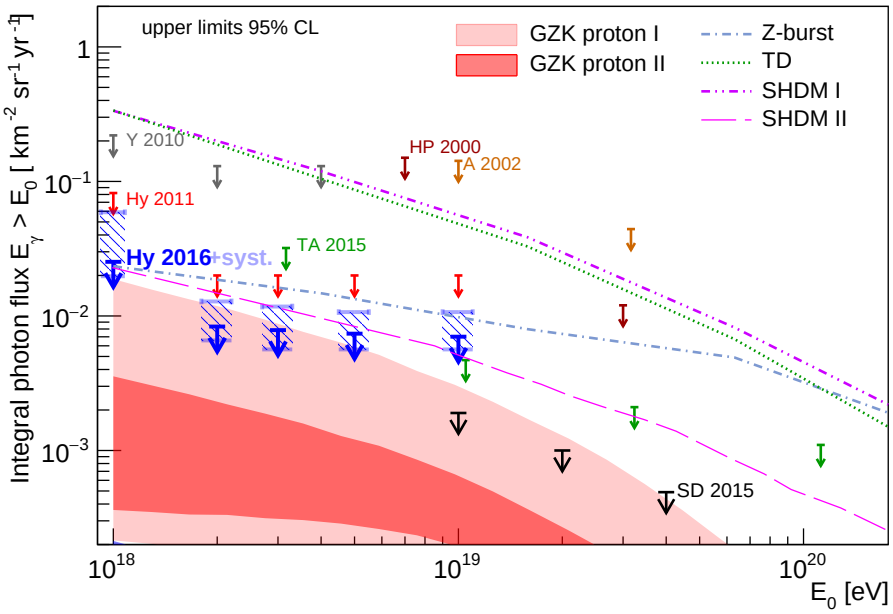

Figure 10: Upper limits on the integrated photon flux, along with several model predictions [46, 43]. The bold arrows (Hy 2016) correspond to the most recent data analysis in Auger using hybrid events, the blue dashed boxes mark the systematic uncertainties of this study. The limits of previous studies done by Auger, Hy2011 (red arrows), and SD 2015 (black arrows), this last one using only SD data, are also shown. The results from other experiments are also presented in the figure, namely: Telescope Array (TA 2015), Yakutsk (Y 2010), AGASA (A 2002), and Haverah Park (HP 2000).

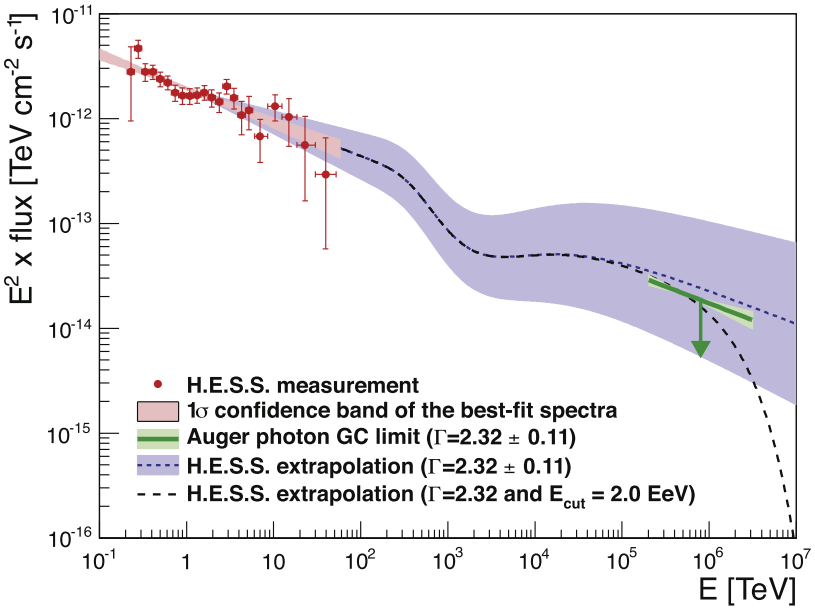

Figure 11: Photon flux as a function of energy from the Galactic center region [43, 46]. The flux measured by H.E.S.S. [47] is shown in red, while the H.E.S.S. extrapolation to the highest energies is represented by the blue dashed line. The thick green line marks the upper limit from Auger given in [43], and the dashed black line shows the spectrum with an exponential cutoff at 2 EeV.

Galactic center region put constraints to the photon flux detected by H.E.S.S. in the TeV range, when extrapolated to EeV energies.

Since there is a close connection between sources of photons and neutrons, Auger also performed complementary searches for neutron candidates and clustering of proton like events around several Galactic sources including the Galactic center and the search results were negative [48, 49].

Neutrinos Neutrino candidates of all flavors can be detected with the SD for events $E > 0.1$ EeV and $\theta > 60^\circ$ [40, 44, 50, 41]. The neutrino searches can be performed either in the Downward Going (DG), or in the Earth-skimming (ES) channels. The DG channel is subdivided into two regimes, the Downward Going Low (DGL), which is used for events with zenith angles 60° to 75°, and the Downward Going High (DGH) for $75^\circ < \theta < 90^\circ$. Finally, the ES channel applies for events in the zenith angle range $90^\circ < \theta < 95^\circ$.

Given the very low cross section of neutrinos, they can interact much deeper in the atmosphere than what is expected for typical hadronic initiated EAS. Thus, neutrino induced showers can be distinguished from the hadronic background by the detection of a broad time structure in the water-Cherenkov detectors, due to the presence of a large electromagnetic component, typical to the one of a "young" shower, whereas the time traces from inclined hadronic events are narrow and are dominated by the muonic component. The separability of the neutrino signals is based on the value of the Area-over-Peak (AoP) of the triggered stations, a variable which relates the time width of the signal measured by each SD station with the maximum height of that signal. In the DG channels, neutrino searches use a Fisher discriminant which combines up to 10 variables using the AoP of 4 (4 or 5) early (central) stations in the DGH (DGL) selections as described in detail in [41]. The ES channel is only sensitive to tau neutrinos, and it is the most sensitive channel. It requires a minimum of three stations, a high eccentricity of the elliptic shape of the triggered area on the ground, and an apparent speed of the trigger times between station pairs with an average value very close to the speed of light, and a small spread. In Figure 12 is shown the discrimination of neutrino shower candidates from the hadronic background using the AoP of time traces for the Earth-skimming channel.

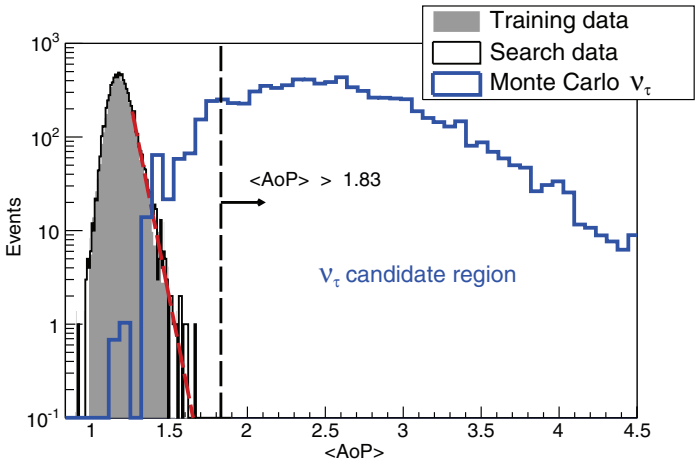

Figure 12: The cut in $\langle$AoP$\rangle$ (dashed line) ensures that there is less than one background event in 50 years of observation time. The selection efficiency for the Earth-skimming channel is 95% [41].

In Figure 13 are shown the results for the integrated and diffusive neutrino fluxes for Auger data ranging from 1 January 2004 to 31 March 2017.

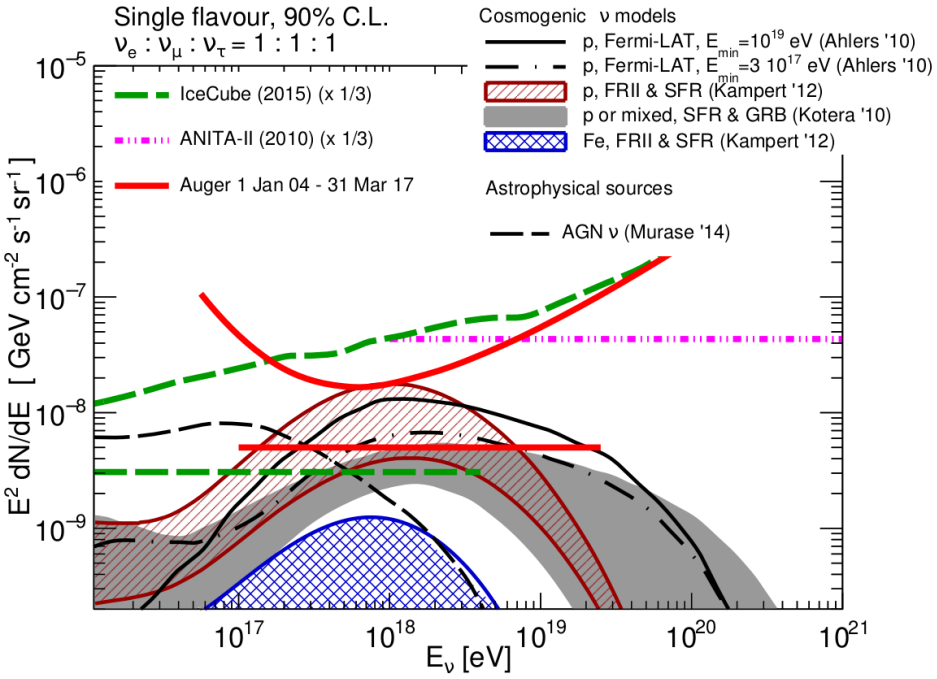

Figure 13: Integral upper limit (at 90% C. L.) for a diffusive neutrino flux of UHE $\frac{dN}{dE_\nu} = kE^{-2}$ given as a normalization, k (straight red line), and a differential upper limit (curved red line). The limits are drawn for a single flavor, assuming equal flavor ratios. Limits for ANITA (magenta dotted dashed line), and IceCube (green dashed line), along with several model predictions are also shown, see [51] for the complete set of references.

For the Figure 13, two types of bounds were calculated: an integral bound integrating a conventional kE^{-2} neutrino spectrum, giving $k < 5 \times 10^{-9}$ GeV cm^{-2} s^{-1}, and a differential limit, calculated by integrating the neutrino flux over consecutive energy bins of 0.5 in $\log_{10} E_\nu$. This differential limit shows that the SD is sensitive to cosmological neutrinos resulting from interactions of UHE protons with the Cosmic Microwave Background [51].

Finally, in Figures 14 and 15 are shown the results for the point source searches, and the sensitivity to cosmogenic neutrino models, respectively. As it can be seen in Figure 14, with the ES channel it is possible to explore the declination range of $-54.5° < \delta < 59.5°$, and with the DG channel it is possible to increase the declination window to $-84.5° < \delta < 59.5°$. The exposure as a function of the zenith angle of the event can be converted to an average exposure for a given declination, integrating in right ascension. The results in Figure 14 use seven more years of full exposure over the previous results presented in [44]. A flavor ratio of $1 : 1 : 1$ was considered, no neutrino candidates were found [51]. The present search allows to put strong constraints to several models predicting cosmogenic neutrinos in scenarios with proton models with strong source evolution and high redshift of the sources, at a 90% *C. L.*, the red area in Figure 15.

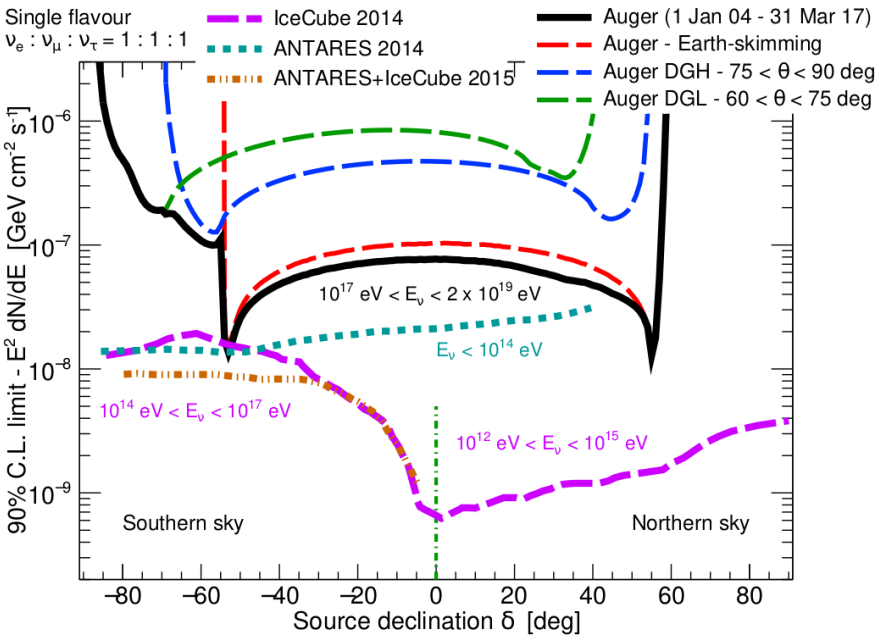

Figure 14: Upper limits at 90% *C. L.* for k^{PS}, where PS stands for Point Source, as a function of the source declination for all the three neutrino channels; Downward Going Low (dashed green), Downward Going High (dashed blue), and Earth-skimming (dashed red). The total exposure is shown in black [51]. The sensitivities for IceCube, Antares and a combination of both are also represented in the figure. Note the different energy ranges of the three detectors.

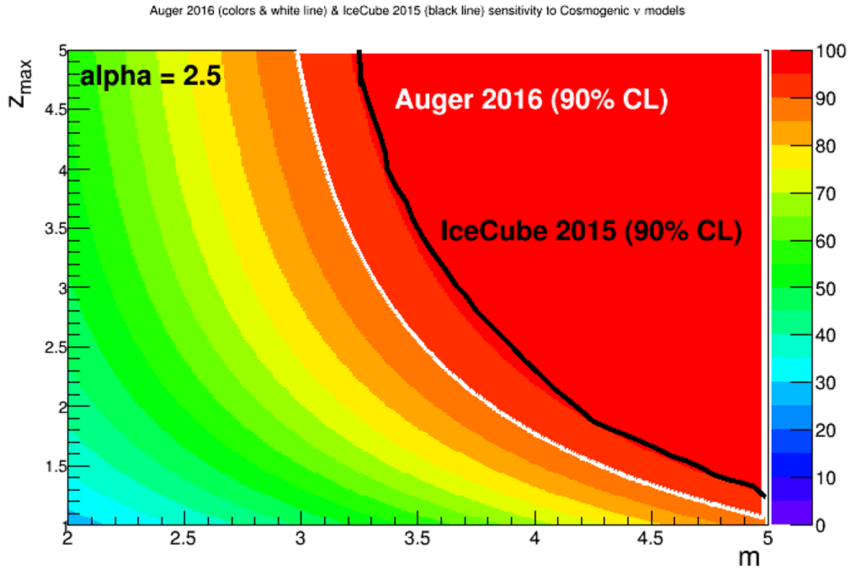

Figure 15: Constraints on the parameter space for cosmological neutrinos in proton models (assuming $dN/dE \propto E^{-2.5}$) as a function of the source evolution m, and maximum redshift of the sources $z_{\rm max}$. The color code represents the confidence levels of exclusion. The region above the white (black) line marks the 90% *C.L.* exclusion limits calculated by Auger (IceCube) [51].

3.4 Multi-messenger astronomy

The Pierre Auger Observatory actively participates in multi-messenger searches in collaboration with other experiments. So far, searches of correlation of the arrival direction of cosmic rays detected by the Telescope Array and Auger collaborations, with the arrival directions of neutrino events detected by IceCube was performed. However, the detection of the first Gravitational Wave (GW) transient GW150914 on September 14, 2015, by the Advanced LIGO detectors opened a new era in multi-messenger astronomy [52], enhancing the participation of many other experiments, of which, the Pierre Auger Observatory is also part.

In [53], a small excess of pairs of high-energy neutrino-induced muon tracks detected by IceCube and the arrival direction of UHECR coming from the hot-spot region reported by Telescope Array, and from the regions close to the super-galactic plane, was reported. Although this excess is not yet significative, the evolution of this signal will be studied with time.

Auger performed neutrino searches in coincidence with the gravitational wave events GW150914, GW151226, LVT15012 [54], and GW170817/GRB 179817A [55]. Below are presented the Auger results for the GW170817/GRB 179817A [56], a gravitational wave event detected on August 17, 2017, later observed as a short gamma-ray burst by the Fermi-GBM and INTEGRAL. This event was caused by the merging of a binary of neutron stars in the host galaxy NGC 4993, at a distance of ~ 40 Mpc, the closest gravitational event detected so far. Neutrino searches related to this event were carried by the three most sensitive neutrino observatories Ice Cube, Antares and Auger. The sky map of these neutrino searches is shown in Figure 16.

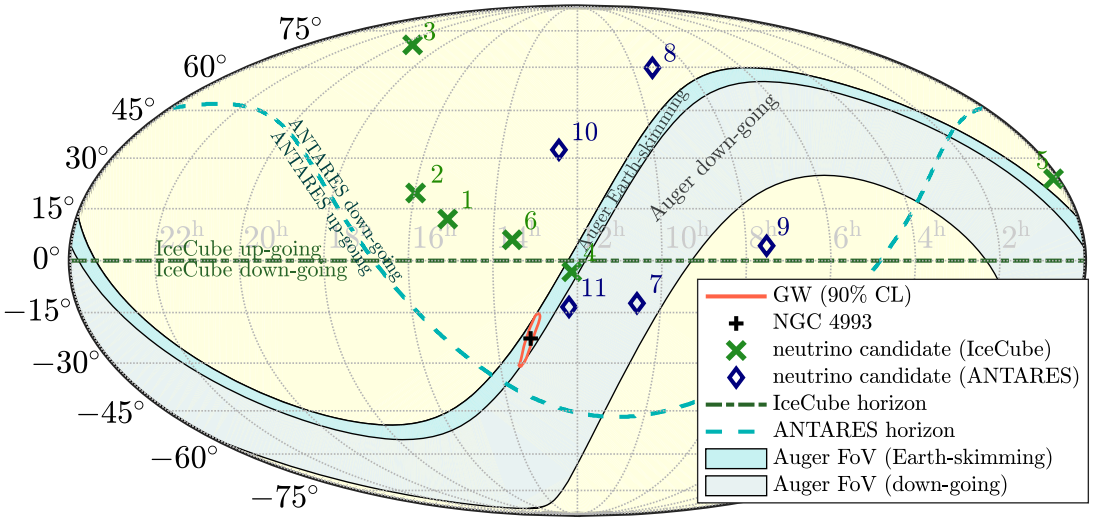

Figure 16: Sensitive sky areas of ANTARES, IceCube and Auger at the time of the GW170817 event in Equatorial Coordinates. The red contour marks the 90% C.L. location of the GW170817 event [52, 55].

The three neutrino observatories are complementary in the energy region, allowing to search for neutrinos in the energy region of $\sim 10^{11}$ eV to $\sim 10^{20}$ eV, as well as for MeV neutrinos with IceCube. The neutrino searches were performed in two time windows; one of ± 500 s, centered at the merger time of the event, and the other one covered the next 14 days after the gravitational wave event. The results for all the neutrino observatories, along with some model predictions for the neutrino emission scaled to a distance of 40 Mpc are shown in Figure 17.

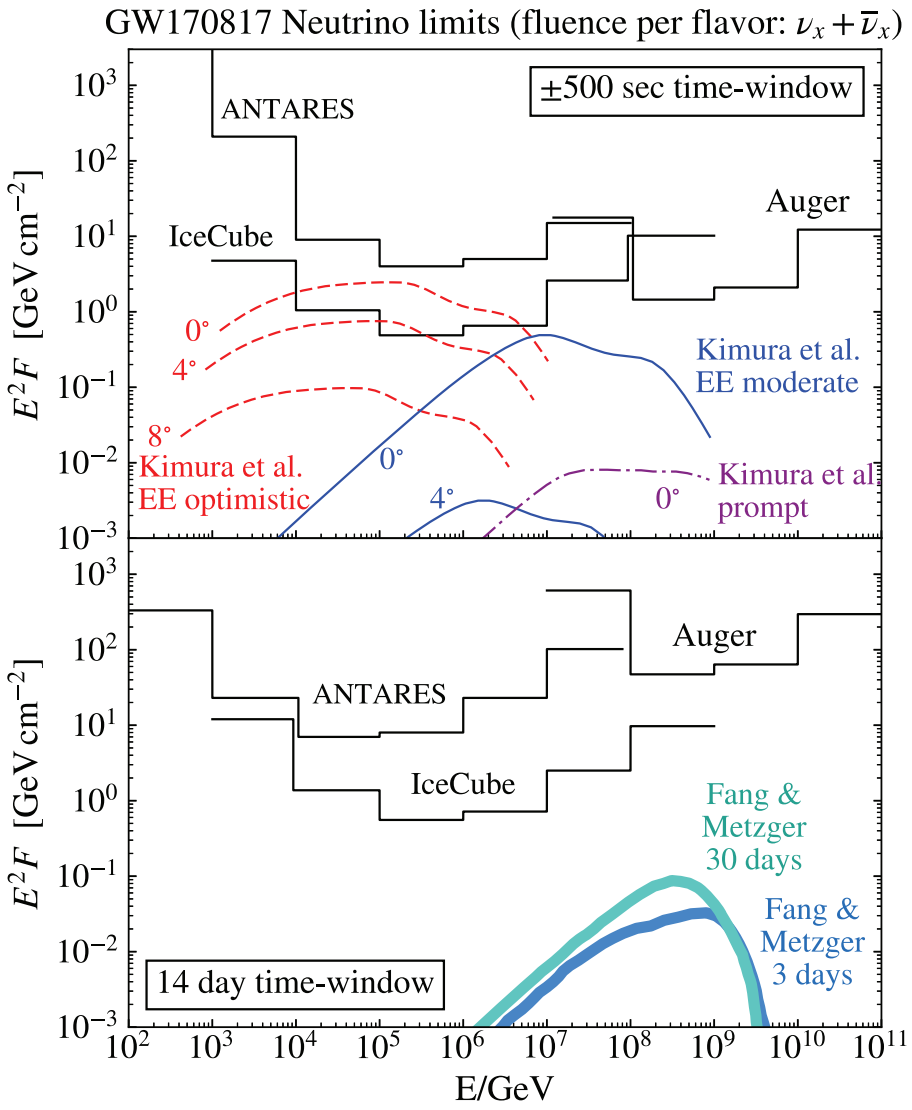

Figure 17: Upper limits at 90% C.L. of the neutrino spectral fluence from GW170817 event for a ±500 s time window (top panel) and in the following 14 days after the trigger (bottom panel) [55].

In Auger, the whole ±500 s time window was observed in the Earth-skimming channel field of view, the most sensitive channel to UHE neutrinos. In this period, the source of GW170817 transited from $\theta \sim 93°.3$ to $\theta \sim 90°.4$ as seen from the center of the array. During this period, the performance of the SD array (which is monitored each minute) was very stable, with an average number of active stations amounting to $\sim 95.8\% \pm 0.1\%$. No inclined showers passing the Earth-skimming channel selection were detected during this period. The estimated number of background events in this 1000 s window is $\sim 6.3 \times 10^{-7}$, for the cuts applied in the Earth-skimming channel [41]. Assuming neutrinos are emitted steadily during this period, with an energy spectrum of E^{-2} [54], the non detection of candidates allow us to put limits to its fluence. In the following 14 days, searches were done both in the Earth-skimming (ES) and Downward Going (DG) channels. From the Auger coordinates, the zenith angle of the optical counterpart of the event oscillates daily

between $\theta \sim 11^\circ$ to $\theta \sim 121^\circ$. The source is visible in the ES channel for $\sim 4\%$ ($90^\circ < \theta < 95^\circ$) of the day, in the DGL channel for $\sim 10.5\%$ ($60^\circ < \theta < 75^\circ$), and in the DGH for 11.1% ($75^\circ < \theta < 90^\circ$). No neutrino candidates were found in this time window as well. No significative counterpart was found in any of the searches with any of the observatories, a result which is compatible with the expectations of a GRB observed off-axis.

4. AugerPrime

Taking stable data since 2004, the Pierre Auger Observatory published many results about the properties of UHECRs. Among the latest results at the highest energies, using SD data, it was established the extragalactic origin of cosmic rays with $E > 8\,\mathrm{EeV}$ [22]. However, to identify the UHECR sources, it is crucial to determine the nuclear mass composition in the flux suppression energy region. Unfortunately, the low duty cycle of the FD does not allow a significant data sample for energies above $10^{19.6}$ eV [5]. Several other mass composition analysis using the SD are performed by the Pierre Auger Collaboration, but these suffer from larger systematic uncertainties due to the uncertainties in the assessment of muon content of the shower using the water-Cherenkov detectors.

To address such challenges, the Pierre Auger Observatory is currently undergoing a major upgrade phase, called AugerPrime, aimed at enhancing the determination of the nuclear mass composition of cosmic rays, event-by-event, reaching a sensitivity as small as 10% for a proton flux at energies close to the flux suppression region with almost doubled statistics [57]. The key upgrade consists in the installation of a $4\,\mathrm{m}^2$ plastic scintillator detector on top of each one of the 1660 water-Cherenkov stations, enabling a better discrimination between the electromagnetic and muonic components of the shower. Additionally, the duty cycle of the fluorescence telescopes will be extended, allowing a direct determination of the depth of the shower maximum with increased statistics at the highest energies. The electronics of the Surface Detector stations is being upgraded to have an increased sampling rate and a better timing accuracy, as well as a higher dynamic range, allowing a better reconstruction of the geometry of the showers. The study of hadronic interactions will benefit from the deployment of an array of buried muon counters in the 750 m array, from which an independent and direct estimation of the muon content of extensive air showers can be done for energies $10^{17.5}$ to 10^{19} eV, encompassing the ankle region and almost overlapping with the energies attained at the LHC. AugerPrime will collect data until 2025.

5. Acknowledgments

The successful installation, commissioning, and operation of the Pierre Auger Observatory would not have been possible without the strong commitment and effort from the technical and administrative staff in Malargüe, and the financial support from a number of funding agencies in the participating countries, listed at https://www.auger.org/index.php/about-us/funding-agencies. The author was supported by the European Union Operation Fund project CZ.02.1.01/0.0/0.0/16013/0001402.

References

[1] R. Aloisio, V. Berezinsky and A. Gazizov, "Transition from galactic to extragalactic cosmic rays," Astropart. Phys. **39-40** (2012) 129

[2] The Telescope Array Collaboration, "The surface detector array of the Telescope Array experiment," Nucl. Instrum. Meth. A **689** (2013) 87.

[3] The Pierre Auger Collaboration, "The Pierre Auger Cosmic Ray Observatory," Nucl. Instrum. Meth. A **798** (2015) 172.

[4] The Pierre Auger Collaboration, "Depth of maximum of air-shower profiles at the Pierre Auger Observatory. I. Measurements at energies above $10^{17.8}$ eV," Phys. Rev. D **90** (2014) no.12, 122005.

[5] J. Bellido, for the Pierre Auger Collaboration 2017, Proc. 35th Int. Cosmic Ray Conf., PoS (ICRC 2017)506.

[6] T. Bergmann, R. Engel, D. Heck, N. N. Kalmykov, S. Ostapchenko, T. Pierog, T. Thouw and K. Werner, "One-dimensional Hybrid Approach to Extensive Air Shower Simulation," Astropart. Phys. **26** (2007) 420.

[7] T. Pierog, I. Karpenko, J. M. Katzy, E. Yatsenko and K. Werner, "EPOS LHC: Test of collective hadronization with data measured at the CERN Large Hadron Collider," Phys. Rev. C **92** (2015) no.3, 034906.

[8] S. Ostapchenko, "Monte Carlo treatment of hadronic interactions in enhanced Pomeron scheme: I. QGSJET-II model," Phys. Rev. D **83** (2011) 014018; S. Ostapchenko, "LHC data on inelastic diffraction and uncertainties in the predictions for longitudinal extensive air shower development," Phys. Rev. D **89** (2014) no.7, 074009.

[9] F. Riehn, Diss. University Karlsruhe (2015); F. Riehn et al., Proc. 34th Int. Cosmic Ray Conf., PoS (ICRC 2015)558.

[10] S. Blaess, J. Bellido, and B. Dawson, Proc. 35th Int. Cosmic Ray Conf., PoS (ICRC 2017)490.

[11] The Pierre Auger Collaboration, "Inferences on mass composition and tests of hadronic interactions from 0.3 to 100 EeV using the water-Cherenkov detectors of the Pierre Auger Observatory," Phys. Rev. D **96** (2017) no.12, 122003.

[12] P. Sanchéz-Lucas, for the Pierre Auger Collaboration 2017, Proc. 35th Int. Cosmic Ray Conf., PoS (ICRC 2017)495.

[13] The Pierre Auger Collaboration, "Reconstruction of inclined air showers detected with the Pierre Auger Observatory," JCAP **1408** (2014) no.08, 019

[14] The Pierre Auger Collaboration, "The effect of the geomagnetic field on cosmic ray energy estimates and large scale anisotropy searches on data from the Pierre Auger Observatory," JCAP **1111** (2011) 022

[15] The Pierre Auger Collaboration, "Impact of Atmospheric Effects on the Energy Reconstruction of Air Showers Observed by the Surface Detectors of the Pierre Auger Observatory," JINST **12** (2017) no.02, P02006

[16] The Pierre Auger Collaboration, "Trigger and aperture of the surface detector array of the Pierre Auger Observatory," Nucl. Instrum. Meth. A **613** (2010) 29

[17] V. Verzi, for the Pierre Auger Collaboration 2013, Proc. 33th Int. Cosmic Ray Conf., (ICRC 2013) p.0928.

[18] The Pierre Auger Collaboration, "Search for First Harmonic Modulation in the Right Ascension Distribution of Cosmic Rays Detected at the Pierre Auger Observatory," Astropart. Phys. **34** (2011) 627

[19] The Pierre Auger Collaboration, "Large scale distribution of arrival directions of cosmic rays detected above 10^{18} eV at the Pierre Auger Observatory," Astrophys. J. Suppl. **203** (2012) 34

[20] The Pierre Auger Collaboration, "Large Scale Distribution of Ultra High Energy Cosmic Rays Detected at the Pierre Auger Observatory With Zenith Angles up to 80°," Astrophys. J. **802** (2015) no.2, 111

[21] O. Taborda, for the Pierre Auger Collaboration 2017, Proc. 35th Int. Cosmic Ray Conf., PoS (ICRC 2017)523.

[22] The Pierre Auger Collaboration, "Observation of a Large-scale Anisotropy in the Arrival Directions of Cosmic Rays above 8×10^{18} eV," Science **357** (2017) no.6537, 1266.

[23] J. Linsley, "Fluctuation effects on directional data," Phys. Rev. Lett. **34** (1975) 1530.

[24] R. Jansson and G. R. Farrar, "A New Model of the Galactic Magnetic Field," Astrophys. J. **757** (2012) 14

[25] A. H. Compton and I. A. Getting, "An Apparent Effect of Galactic Rotation on the Intensity of Cosmic Rays," Phys. Rev. **47** (1935) no.11, 817.

[26] M. Kachelriess and P. D. Serpico, "The Compton-Getting effect on ultra-high energy cosmic rays of cosmological origin," Phys. Lett. B **640** (2006) 225

[27] C. D. Dermer and S. Razzaque, "Acceleration of Ultra-High Energy Cosmic Rays in the Colliding Shells of Blazars and GRBs: Constraints from the Fermi Gamma ray Space Telescope," Astrophys. J. **724** (2010) 1366

[28] M. Unger, G. R. Farrar and L. A. Anchordoqui, "Origin of the ankle in the ultrahigh energy cosmic ray spectrum, and of the extragalactic protons below it," Phys. Rev. D **92** (2015) no.12, 123001

[29] U. Giaccari, for the Pierre Auger Collaboration 2017, Proc. 35th Int. Cosmic Ray Conf., PoS (ICRC 2017)483.

[30] The Pierre Auger Collaboration, "An Indication of anisotropy in arrival directions of ultra-high-energy cosmic rays through comparison to the flux pattern of extragalactic gamma-ray sources," Astrophys. J. **853** (2018) no.2, L29.

[31] The Fermi-LAT Collaboration, "2FHL: The Second Catalog of Hard Fermi-LAT Sources," Astrophys. J. Suppl. **222** (2016) no.1, 5

[32] The Fermi-LAT Collaboration, "GeV Observations of Star-forming Galaxies with *Fermi* LAT," Astrophys. J. **755** (2012) 164

[33] The Pierre Auger Collaboration, "Combined fit of spectrum and composition data as measured by the Pierre Auger Observatory," JCAP **1704** (2017) no.04, 038 Erratum: [JCAP **1803** (2018) no.03, E02]

[34] K. Greisen, "End to the cosmic ray spectrum?," Phys. Rev. Lett. **16** (1966) 748.

[35] G. T. Zatsepin and V. A. Kuzmin, "Upper limit of the spectrum of cosmic rays," JETP Lett. **4** (1966) 78 [Pisma Zh. Eksp. Teor. Fiz. **4** (1966) 114].

[36] V. S. Berezinsky and G. T. Zatsepin, "Cosmic rays at ultrahigh-energies (neutrino?)," Phys. Lett. **28B** (1969) 423.

[37] F. Halzen and D. Hooper, "High-energy neutrino astronomy: The Cosmic ray connection," Rept. Prog. Phys. **65** (2002) 1025

[38] C. Bleve, for the Pierre Auger Collaboration 2015, Proc. 34th Int. Cosmic Ray Conf., PoS (ICRC 2015)1103.

[39] The Pierre Auger Collaboration, "Search for photons with energies above 10^{18} eV using the hybrid detector of the Pierre Auger Observatory," JCAP **1704** (2017) no.04, 009.

[40] The Pierre Auger Collaboration, "A Search for Ultra-High Energy Neutrinos in Highly Inclined Events at the Pierre Auger Observatory," Phys. Rev. D **84** (2011) 122005. Erratum: [Phys. Rev. D **84** (2011) 029902]

[41] The Pierre Auger Collaboration, "Improved limit to the diffuse flux of ultrahigh energy neutrinos from the Pierre Auger Observatory," Phys. Rev. D **91** (2015) no.9, 092008.

[42] The Pierre Auger Collaboration, "A search for point sources of EeV photons," Astrophys. J. **789** (2014) no.2, 160.

[43] The Pierre Auger Collaboration, "A targeted search for point sources of EeV photons with the Pierre Auger Observatory," Astrophys. J. **837** (2017) no.2, L25.

[44] The Pierre Auger Collaboration, "Search for point-like sources of ultra-high energy neutrinos at the Pierre Auger Observatory and improved limit on the diffuse flux of tau neutrinos," Astrophys. J. **755** (2012) L4.

[45] P. Homola, M. Risse, R. Engel, D. Gora, J. Pekala, B. Wilczynska and H. Wilczynski, "Characteristics of geomagnetic cascading of ultrahigh energy photons at the southern and northern sites of the Pierre Auger Observatory," Astropart. Phys. **27** (2007) 174

[46] M. Niechciol, for the Pierre Auger Collaboration 2017, Proc. 35th Int. Cosmic Ray Conf., PoS (ICRC 2017)517.

[47] The H.E.S.S. Collaboration, "Acceleration of petaelectronvolt protons in the Galactic Centre," Nature **531** (2016) 476

[48] The Pierre Auger Collaboration, "A Targeted Search for Point Sources of EeV Neutrons," Astrophys. J. **789** (2014) L34.

[49] The Pierre Auger Collaboration, "A Search for Point Sources of EeV Neutrons," Astrophys. J. **760** (2012) 148.

[50] The Pierre Auger Collaboration, "Ultrahigh Energy Neutrinos at the Pierre Auger Observatory," Adv. High Energy Phys. **2013** (2013) 708680.

[51] E. Zas, for the Pierre Auger Collaboration 2017, Proc. 35th Int. Cosmic Ray Conf., PoS (ICRC 2017)972.

[52] LIGO Scientific and Virgo Collaborations, "Observation of Gravitational Waves from a Binary Black Hole Merger," Phys. Rev. Lett. **116** (2016) no.6, 061102.

[53] IceCube and Pierre Auger and Telescope Array Collaborations, "Search for correlations between the arrival directions of IceCube neutrino events and ultrahigh-energy cosmic rays detected by the Pierre Auger Observatory and the Telescope Array," JCAP **1601** (2016) no.01, 037.

[54] The Pierre Auger Collaboration, "Ultrahigh-energy neutrino follow-up of gravitational wave events GW150914 and GW151226 with the Pierre Auger Observatory," Phys. Rev. D **94** (2016) no.12, 122007.

[55] ANTARES and IceCube and Pierre Auger and LIGO Scientific and Virgo Collaborations, "Search for High-energy Neutrinos from Binary Neutron Star Merger GW170817 with ANTARES, IceCube, and the Pierre Auger Observatory," Astrophys. J. **850** (2017) no.2, L35.

[56] B. P. Abbott *et al.*, "Multi-messenger Observations of a Binary Neutron Star Merger," Astrophys. J. **848** (2017) no.2, L12.

[57] The Pierre Auger Collaboration, "The Pierre Auger Observatory Upgrade - Preliminary Design Report," arXiv:1604.03637 [astro-ph.IM].

DISCUSSION

WOLFGANG KUNDT: From the anisotropy of their arrivals, you concluded at an extragalactic origin of the highest energy CRs. In Francos's workshop proceedings of 2009, 2010 and 2014, I came to the opposite conclusion.

EVA SANTOS: Dear Wolfgang Kundt, unfortunately your references to the Franco's workshop proceedings are too vague to give a specific comment relative to them. The dipole anisotropy found by Auger for cosmic rays with $E > 8\,\mathrm{EeV}$ in [22] is the first and only evidence for the extragalactic origin of UHECR. In the past, none of the experimental results reached sufficient statistics to claim about the origin of these cosmic rays with a high level of significance. In other works Auger also conducted searches for excesses of events coming from the Galactic center but no significant excess was observed at the highest energies.

JIM BEAL: Can you say a bit more about the Auger signal from the direction of Cen A?

EVA SANTOS: Dear Jim Beal, according to our most recent data from [29], using events up to April 30 2017, the most significative excess in the direction of Cen A occurs for $E > 58\,\mathrm{EeV}$ in an angular window of 15°, where a minimum value of the cumulative binomial probability was found to be $P = 1.1 \times 10^{-5}$. A total of 19 events were observed in this angular window whereas ~ 6 events were expected on average from an isotropic flux hypothesis. After penalizing for the energy scan and angle scan, this corresponds to a statistical significance of $3.1\,\sigma$.

In [30] is reported the most significative evidence for anisotropy of UHECR at the intermediate angular scale. In this case, the correlation of the arrival directions of events with $E > 20\,\mathrm{EeV}$ coming from zenith angles $\theta < 80^\circ$ is studied considering two populations of nearby extragalactic gamma-ray sources: starburst galaxies and AGNs. For starburst galaxies, a 4σ deviation from isotropy is found for $E > 39\,\mathrm{EeV}$ for an angular scale of 13°, while for AGNs, a 2.7σ deviation is found for events with $E > 60\,\mathrm{EeV}$ in an angular scale of 7°, where the gamma-AGN signal is dominated by Centaurus A.

The Pierre Auger Collaboration

A. Aab[75], P. Abreu[67], M. Aglietta[49,48], I.F.M. Albuquerque[18], J.M. Albury[12], I. Allekotte[1], A. Almela[8,11], J. Alvarez Castillo[63], J. Alvarez-Muñiz[74], G.A. Anastasi[40,42], L. Anchordoqui[81], B. Andrada[8], S. Andringa[67], C. Aramo[46], N. Arsene[69], H. Asorey[1,26], P. Assis[67], G. Avila[9,10], A.M. Badescu[70], A. Balaceanu[68], F. Barbato[56,46], R.J. Barreira Luz[67], S. Baur[35], K.H. Becker[33], J.A. Bellido[12], C. Berat[32], M.E. Bertaina[58,48], X. Bertou[1], P.L. Biermann[b], J. Biteau[30], S.G. Blaess[12], A. Blanco[67], J. Blazek[28], C. Bleve[52,44], M. Boháčová[28], C. Bonifazi[23], N. Borodai[64], A.M. Botti[8,35], J. Brack[f], T. Bretz[37], A. Bridgeman[34], F.L. Briechle[37], P. Buchholz[39], A. Bueno[73], S. Buitink[75], M. Buscemi[54,43], K.S. Caballero-Mora[62], L. Caccianiga[55], L. Calcagni[4], A. Cancio[11,8], F. Canfora[75,77], J.M. Carceller[73], R. Caruso[54,43], A. Castellina[49,48], F. Catalani[16], G. Cataldi[44], L. Cazon[67], J.A. Chinellato[19], J. Chudoba[28], L. Chytka[29], R.W. Clay[12], A.C. Cobos Cerutti[7], R. Colalillo[56,46], A. Coleman[86], L. Collica[48], M.R. Coluccia[52,44], R. Conceição[67], G. Consolati[45,50], F. Contreras[9,10], M.J. Cooper[12], S. Coutu[86], C.E. Covault[79], S. D'Amico[51,44], B. Daniel[19], S. Dasso[5,3], K. Daumiller[35], B.R. Dawson[12], J.A. Day[12], R.M. de Almeida[25], S.J. de Jong[75,77], G. De Mauro[75,77], J.R.T. de Mello Neto[23,24], I. De Mitri[40,42], J. de Oliveira[25], V. de Souza[17], J. Debatin[34], O. Deligny[30], N. Dhital[64], M.L. Díaz Castro[19], F. Diogo[67], C. Dobrigkeit[19], J.C. D'Olivo[63], Q. Dorosti[39], R.C. dos Anjos[22], M.T. Dova[4], A. Dundovic[38], J. Ebr[28], R. Engel[35], M. Erdmann[37], C.O. Escobar[d], A. Etchegoyen[8,11], H. Falcke[75,78,77], J. Farmer[87], G. Farrar[84], A.C. Fauth[19], N. Fazzini[d], F. Feldbusch[36], F. Fenu[58,48], L.P. Ferreyro[8], B. Fick[83], J.M. Figueira[8], A. Filipčič[72,71], M.M. Freire[6], T. Fujii[87,g], A. Fuster[8,11], R. Gaïor[31], B. García[7], H. Gemmeke[36], A. Gherghel-Lascu[68], P.L. Ghia[30], U. Giaccari[23,14], M. Giammarchi[45], M. Giller[65], D. Głas[66], C. Glaser[37], J. Glombitza[37], G. Golup[1], M. Gómez Berisso[1], P.F. Gómez Vitale[9,10], N. González[8], I. Goos[1,35], D. Góra[64], A. Gorgi[49,48], M. Gottowik[33], T.D. Grubb[12], F. Guarino[56,46], G.P. Guedes[20], E. Guido[48,58], R. Halliday[79], M.R. Hampel[8], P. Hansen[4], D. Harari[1], T.A. Harrison[12], V.M. Harvey[12], A. Haungs[35], T. Hebbeker[37], D. Heck[35], P. Heimann[39], G.C. Hill[12], C. Hojvat[d], E.M. Holt[34,8], P. Homola[64], J.R. Hörandel[75,77], P. Horvath[29], M. Hrabovský[29], T. Huege[35,c], J. Hulsman[8,35], A. Insolia[54,43], P.G. Isar[69], I. Jandt[33], J.A. Johnsen[80], M. Josebachuili[8], J. Jurysek[28], A. Kääpä[33], K.H. Kampert[33], B. Keilhauer[35], N. Kemmerich[18], J. Kemp[37], H.O. Klages[35], M. Kleifges[36], J. Kleinfeller[9], R. Krause[37], D. Kuempel[33], G. Kukec Mezek[71], N. Kunka[36], A. Kuotb Awad[34], B.L. Lago[15], D. LaHurd[79], R.G. Lang[17], R. Legumina[65], M.A. Leigui de Oliveira[21], V. Lenok[35], A. Letessier-Selvon[31], I. Lhenry-Yvon[30], D. Lo Presti[54,43], L. Lopes[67], R. López[59], A. López Casado[74], R. Lorek[79], Q. Luce[30], A. Lucero[8], M. Malacari[87], M. Mallamaci[55,45], D. Mandat[28], P. Mantsch[d], A.G. Mariazzi[4], I.C. Mariş[13], G. Marsella[52,44], D. Martello[52,44], H. Martinez[60], O. Martínez Bravo[59], H.J. Mathes[35], S. Mathys[33], J. Matthews[82], G. Matthiae[57,47], E. Mayotte[33], P.O. Mazur[d], C. Medina[80], G. Medina-Tanco[63], D. Melo[8], A. Menshikov[36], K.-D. Merenda[80], S. Michal[29], M.I. Micheletti[6], L. Middendorf[37], L. Miramonti[55,45], B. Mitrica[68], D. Mockler[34], S. Mollerach[1], F. Montanet[32], C. Morello[49,48], G. Morlino[40,42], M. Mostafá[86], A.L. Müller[8,35], M.A. Muller[19,e], S. Müller[34,8], R. Mussa[48], L. Nellen[63], P.H. Nguyen[12], M. Niculescu-Oglinzanu[68], M. Niechciol[39], L. Niemietz[33], D. Nitz[83,h], D. Nosek[27], V. Novotny[27], L. Nožka[29], A Nucita[52,44], L.A. Núñez[26], F. Oikonomou[86], A. Olinto[87], M. Palatka[28], J. Pallotta[2], P. Papenbreer[33], G. Parente[74], A. Parra[59], T. Paul[81], M. Pech[28], F. Pedreira[74], J. Pękala[64], R. Pelayo[61], J. Peña-Rodriguez[26], L.A.S. Pereira[19], M. Perlin[8], L. Perrone[52,44], C. Peters[37], S. Petrera[40,42], J. Phuntsok[86], T. Pierog[35], M. Pimenta[67], V. Pirronello[54,43], M. Platino[8], J. Poh[87], B. Pont[75], C. Porowski[64], R.R. Prado[17], P. Privitera[87], M. Prouza[28], A. Puyleart[83], E.J. Quel[2], S. Querchfeld[33], S. Quinn[79], R. Ramos-Pollan[26], J. Rautenberg[33], D. Ravignani[8], M. Reininghaus[35], J. Ridky[28], F. Riehn[67], M. Risse[39], P. Ristori[2], V. Rizi[53,42], W. Rodrigues de Carvalho[18], G. Rodriguez Fernandez[57,47], J. Rodriguez Rojo[9], M.J. Roncoroni[8], M. Roth[35], E. Roulet[1], A.C. Rovero[5], P. Ruehl[39], S.J. Saffi[12], A. Saftoiu[68], F. Salamida[53,42], H. Salazar[59], A. Saleh[71], G. Salina[47], F. Sánchez[8], P. Sanchez-

Lucas[73], E.M. Santos[18], E. Santos[28], F. Sarazin[80], R. Sarmento[67], C. Sarmiento-Cano[8], R. Sato[9], P. Savina[52,44], M. Schauer[33], V. Scherini[44], H. Schieler[35], M. Schimassek[34], M. Schimp[33], D. Schmidt[35,8], O. Scholten[76,c], P. Schovánek[28], F.G. Schröder[34], S. Schröder[33], A. Schulz[34], J. Schumacher[37], S.J. Sciutto[4], A. Segreto[41,43], R.C. Shellard[14], G. Sigl[38], G. Silli[8,35], O. Sima[68,i], R. Šmída[37], G.R. Snow[88], P. Sommers[86], J.F. Soriano[81], J. Souchard[32], R. Squartini[9], D. Stanca[68], S. Stanič[71], J. Stasielak[64], P. Stassi[32], M. Stolpovskiy[32], F. Strafella[52,44], A. Streich[34], F. Suarez[8,11], M. Suárez-Durán[26], T. Sudholz[12], T. Suomijärvi[30], A.D. Supanitsky[5], J. Šupík[29], J. Swain[85], Z. Szadkowski[66], A. Taboada[35], O.A. Taborda[1], C. Timmermans[77,75], C.J. Todero Peixoto[16], B. Tomé[67], G. Torralba Elipe[74], P. Travnicek[28], M. Trini[71], M. Tueros[4], R. Ulrich[35], M. Unger[35], M. Urban[37], J.F. Valdés Galicia[63], I. Valiño[74], L. Valore[56,46], P. van Bodegom[12], A.M. van den Berg[76], A. van Vliet[75], E. Varela[59], B. Vargas Cárdenas[63], R.A. Vázquez[74], D. Veberič[35], C. Ventura[24], I.D. Vergara Quispe[4], V. Verzi[47], J. Vicha[28], L. Villaseñor[59], S. Vorobiov[71], H. Wahlberg[4], O. Wainberg[8,11], D. Walz[37], A.A. Watson[a], M. Weber[36], A. Weindl[35], M. Wiedeński[66], L. Wiencke[80], H. Wilczyński[64], M. Wirtz[37], D. Wittkowski[33], B. Wundheiler[8], L. Yang[71], A. Yushkov[28], E. Zas[74], D. Zavrtanik[71,72], M. Zavrtanik[72,71], L. Zehrer[71], A. Zepeda[60], B. Zimmermann[36], M. Ziolkowski[39], Z. Zong[30], F. Zuccarello[54,43]

— • —

[1] Centro Atómico Bariloche and Instituto Balseiro (CNEA-UNCuyo-CONICET), San Carlos de Bariloche, Argentina
[2] Centro de Investigaciones en Láseres y Aplicaciones, CITEDEF and CONICET, Villa Martelli, Argentina
[3] Departamento de Física and Departamento de Ciencias de la Atmósfera y los Océanos, FCEyN, Universidad de Buenos Aires and CONICET, Buenos Aires, Argentina
[4] IFLP, Universidad Nacional de La Plata and CONICET, La Plata, Argentina
[5] Instituto de Astronomía y Física del Espacio (IAFE, CONICET-UBA), Buenos Aires, Argentina
[6] Instituto de Física de Rosario (IFIR) - CONICET/U.N.R. and Facultad de Ciencias Bioquímicas y Farmacéuticas U.N.R., Rosario, Argentina
[7] Instituto de Tecnologías en Detección y Astropartículas (CNEA, CONICET, UNSAM), and Universidad Tecnológica Nacional - Facultad Regional Mendoza (CONICET/CNEA), Mendoza, Argentina
[8] Instituto de Tecnologías en Detección y Astropartículas (CNEA, CONICET, UNSAM), Buenos Aires, Argentina
[9] Observatorio Pierre Auger, Malargüe, Argentina
[10] Observatorio Pierre Auger and Comisión Nacional de Energía Atómica, Malargüe, Argentina
[11] Universidad Tecnológica Nacional - Facultad Regional Buenos Aires, Buenos Aires, Argentina
[12] University of Adelaide, Adelaide, S.A., Australia
[13] Université Libre de Bruxelles (ULB), Brussels, Belgium
[14] Centro Brasileiro de Pesquisas Fisicas, Rio de Janeiro, RJ, Brazil
[15] Centro Federal de Educação Tecnológica Celso Suckow da Fonseca, Nova Friburgo, Brazil
[16] Universidade de São Paulo, Escola de Engenharia de Lorena, Lorena, SP, Brazil
[17] Universidade de São Paulo, Instituto de Física de São Carlos, São Carlos, SP, Brazil
[18] Universidade de São Paulo, Instituto de Física, São Paulo, SP, Brazil
[19] Universidade Estadual de Campinas, IFGW, Campinas, SP, Brazil
[20] Universidade Estadual de Feira de Santana, Feira de Santana, Brazil
[21] Universidade Federal do ABC, Santo André, SP, Brazil
[22] Universidade Federal do Paraná, Setor Palotina, Palotina, Brazil
[23] Universidade Federal do Rio de Janeiro, Instituto de Física, Rio de Janeiro, RJ, Brazil
[24] Universidade Federal do Rio de Janeiro (UFRJ), Observatório do Valongo, Rio de Janeiro, RJ, Brazil
[25] Universidade Federal Fluminense, EEIMVR, Volta Redonda, RJ, Brazil
[26] Universidad Industrial de Santander, Bucaramanga, Colombia

[27] Charles University, Faculty of Mathematics and Physics, Institute of Particle and Nuclear Physics, Prague, Czech Republic
[28] Institute of Physics of the Czech Academy of Sciences, Prague, Czech Republic
[29] Palacky University, RCPTM, Olomouc, Czech Republic
[30] Institut de Physique Nucléaire d'Orsay (IPNO), Université Paris-Sud, Univ. Paris/Saclay, CNRS-IN2P3, Orsay, France
[31] Laboratoire de Physique Nucléaire et de Hautes Energies (LPNHE), Universités Paris 6 et Paris 7, CNRS-IN2P3, Paris, France
[32] Univ. Grenoble Alpes, CNRS, Grenoble Institute of Engineering Univ. Grenoble Alpes, LPSC-IN2P3, 38000 Grenoble, France, France
[33] Bergische Universität Wuppertal, Department of Physics, Wuppertal, Germany
[34] Karlsruhe Institute of Technology, Institute for Experimental Particle Physics (ETP), Karlsruhe, Germany
[35] Karlsruhe Institute of Technology, Institut für Kernphysik, Karlsruhe, Germany
[36] Karlsruhe Institute of Technology, Institut für Prozessdatenverarbeitung und Elektronik, Karlsruhe, Germany
[37] RWTH Aachen University, III. Physikalisches Institut A, Aachen, Germany
[38] Universität Hamburg, II. Institut für Theoretische Physik, Hamburg, Germany
[39] Universität Siegen, Fachbereich 7 Physik - Experimentelle Teilchenphysik, Siegen, Germany
[40] Gran Sasso Science Institute, L'Aquila, Italy
[41] INAF - Istituto di Astrofisica Spaziale e Fisica Cosmica di Palermo, Palermo, Italy
[42] INFN Laboratori Nazionali del Gran Sasso, Assergi (L'Aquila), Italy
[43] INFN, Sezione di Catania, Catania, Italy
[44] INFN, Sezione di Lecce, Lecce, Italy
[45] INFN, Sezione di Milano, Milano, Italy
[46] INFN, Sezione di Napoli, Napoli, Italy
[47] INFN, Sezione di Roma "Tor Vergata", Roma, Italy
[48] INFN, Sezione di Torino, Torino, Italy
[49] Osservatorio Astrofisico di Torino (INAF), Torino, Italy
[50] Politecnico di Milano, Dipartimento di Scienze e Tecnologie Aerospaziali , Milano, Italy
[51] Università del Salento, Dipartimento di Ingegneria, Lecce, Italy
[52] Università del Salento, Dipartimento di Matematica e Fisica “E. De Giorgi”, Lecce, Italy
[53] Università dell'Aquila, Dipartimento di Scienze Fisiche e Chimiche, L'Aquila, Italy
[54] Università di Catania, Dipartimento di Fisica e Astronomia, Catania, Italy
[55] Università di Milano, Dipartimento di Fisica, Milano, Italy
[56] Università di Napoli "Federico II", Dipartimento di Fisica “Ettore Pancini“, Napoli, Italy
[57] Università di Roma “Tor Vergata”, Dipartimento di Fisica, Roma, Italy
[58] Università Torino, Dipartimento di Fisica, Torino, Italy
[59] Benemérita Universidad Autónoma de Puebla, Puebla, México
[60] Centro de Investigación y de Estudios Avanzados del IPN (CINVESTAV), México, D.F., México
[61] Unidad Profesional Interdisciplinaria en Ingeniería y Tecnologías Avanzadas del Instituto Politécnico Nacional (UPIITA-IPN), México, D.F., México
[62] Universidad Autónoma de Chiapas, Tuxtla Gutiérrez, Chiapas, México
[63] Universidad Nacional Autónoma de México, México, D.F., México
[64] Institute of Nuclear Physics PAN, Krakow, Poland
[65] University of Łódź, Faculty of Astrophysics, Łódź, Poland
[66] University of Łódź, Faculty of High-Energy Astrophysics,Łódź, Poland
[67] Laboratório de Instrumentação e Física Experimental de Partículas - LIP and Instituto Superior Técnico - IST, Universidade de Lisboa - UL, Lisboa, Portugal

[68] "Horia Hulubei" National Institute for Physics and Nuclear Engineering, Bucharest-Magurele, Romania
[69] Institute of Space Science, Bucharest-Magurele, Romania
[70] University Politehnica of Bucharest, Bucharest, Romania
[71] Center for Astrophysics and Cosmology (CAC), University of Nova Gorica, Nova Gorica, Slovenia
[72] Experimental Particle Physics Department, J. Stefan Institute, Ljubljana, Slovenia
[73] Universidad de Granada and C.A.F.P.E., Granada, Spain
[74] Instituto Galego de Física de Altas Enerxías (I.G.F.A.E.), Universidad de Santiago de Compostela, Santiago de Compostela, Spain
[75] IMAPP, Radboud University Nijmegen, Nijmegen, The Netherlands
[76] KVI - Center for Advanced Radiation Technology, University of Groningen, Groningen, The Netherlands
[77] Nationaal Instituut voor Kernfysica en Hoge Energie Fysica (NIKHEF), Science Park, Amsterdam, The Netherlands
[78] Stichting Astronomisch Onderzoek in Nederland (ASTRON), Dwingeloo, The Netherlands
[79] Case Western Reserve University, Cleveland, OH, USA
[80] Colorado School of Mines, Golden, CO, USA
[81] Department of Physics and Astronomy, Lehman College, City University of New York, Bronx, NY, USA
[82] Louisiana State University, Baton Rouge, LA, USA
[83] Michigan Technological University, Houghton, MI, USA
[84] New York University, New York, NY, USA
[85] Northeastern University, Boston, MA, USA
[86] Pennsylvania State University, University Park, PA, USA
[87] University of Chicago, Enrico Fermi Institute, Chicago, IL, USA
[88] University of Nebraska, Lincoln, NE, USA

———

[a] School of Physics and Astronomy, University of Leeds, Leeds, United Kingdom
[b] Max-Planck-Institut für Radioastronomie, Bonn, Germany
[c] also at Vrije Universiteit Brussel, Brussels, Belgium
[d] Fermi National Accelerator Laboratory, USA
[e] also at Universidade Federal de Alfenas, Poços de Caldas, Brazil
[f] Colorado State University, Fort Collins, CO, USA
[g] now at Institute for Cosmic Ray Research, University of Tokyo
[h] also at Karlsruhe Institute of Technology, Karlsruhe, Germany
[i] also at University of Bucharest, Physics Department, Bucharest, Romania

Acknowledgments

The successful installation, commissioning, and operation of the Pierre Auger Observatory would not have been possible without the strong commitment and effort from the technical and administrative staff in Malargüe. We are very grateful to the following agencies and organizations for financial support:

Argentina – Comisión Nacional de Energía Atómica; Agencia Nacional de Promoción Científica y Tecnológica (ANPCyT); Consejo Nacional de Investigaciones Científicas y Técnicas (CONICET); Gobierno de la Provincia de Mendoza; Municipalidad de Malargüe; NDM Holdings and Valle Las Leñas; in gratitude for their continuing cooperation over land access; Australia – the Australian Research Council; Brazil – Conselho Nacional de Desenvolvimento Científico e Tecnológico (CNPq); Financiadora de Estudos e Projetos (FINEP); Fundação de Amparo à Pesquisa do Estado de Rio de Janeiro (FAPERJ); São Paulo Research Foundation (FAPESP) Grants No. 2010/07359-6 and No. 1999/05404-3; Ministério da Ciência, Tecnologia, Inovações e Comunicações (MCTIC); Czech Republic – Grant No. MSMT CR LG15014, LO1305, LM2015038 and CZ.02.1.01/0.0/0.0/16_013/0001402; France – Centre de Calcul IN2P3/CNRS; Centre National de la Recherche Scientifique (CNRS); Conseil Régional Ile-de-France; Département

Physique Nucléaire et Corpusculaire (PNC-IN2P3/CNRS); Département Sciences de l'Univers (SDU-INSU/CNRS); Institut Lagrange de Paris (ILP) Grant No. LABEX ANR-10-LABX-63 within the Investissements d'Avenir Programme Grant No. ANR-11-IDEX-0004-02; Germany – Bundesministerium für Bildung und Forschung (BMBF); Deutsche Forschungsgemeinschaft (DFG); Finanzministerium Baden-Württemberg; Helmholtz Alliance for Astroparticle Physics (HAP); Helmholtz-Gemeinschaft Deutscher Forschungszentren (HGF); Ministerium für Innovation, Wissenschaft und Forschung des Landes Nordrhein-Westfalen; Ministerium für Wissenschaft, Forschung und Kunst des Landes Baden-Württemberg; Italy – Istituto Nazionale di Fisica Nucleare (INFN); Istituto Nazionale di Astrofisica (INAF); Ministero dell'Istruzione, dell'Universitá e della Ricerca (MIUR); CETEMPS Center of Excellence; Ministero degli Affari Esteri (MAE); Mexico – Consejo Nacional de Ciencia y Tecnología (CONACYT) No. 167733; Universidad Nacional Autónoma de México (UNAM); PAPIIT DGAPA-UNAM; The Netherlands – Ministry of Education, Culture and Science; Netherlands Organisation for Scientific Research (NWO); Dutch national e-infrastructure with the support of SURF Cooperative; Poland – National Centre for Research and Development, Grant No. ERA-NET-ASPERA/02/11; National Science Centre, Grants No. 2013/08/M/ST9/00322, No. 2016/23/B/ST9/01635 and No. HARMONIA 5–2013/10/M/ST9/00062, UMO-2016/22/M/ST9/00198; Portugal – Portuguese national funds and FEDER funds within Programa Operacional Factores de Competitividade through Fundação para a Ciência e a Tecnologia (COMPETE); Romania – Romanian Ministry of Research and Innovation CNCS/CCCDI-UESFISCDI, projects PN-III-P1-1.2-PCCDI-2017-0839/19PCCDI/2018, PN-III-P2-2.1-PED-2016-1922, PN-III-P2-2.1-PED-2016-1659 and PN18090102 within PNCDI III; Slovenia – Slovenian Research Agency; Spain – Comunidad de Madrid; Fondo Europeo de Desarrollo Regional (FEDER) funds; Ministerio de Economía y Competitividad; Xunta de Galicia; European Community 7th Framework Program Grant No. FP7-PEOPLE-2012-IEF-328826; USA – Department of Energy, Contracts No. DE-AC02-07CH11359, No. DE-FR02-04ER41300, No. DE-FG02-99ER41107 and No. DE-SC0011689; National Science Foundation, Grant No. 0450696; The Grainger Foundation; Marie Curie-IRSES/EPLANET; European Particle Physics Latin American Network; European Union 7th Framework Program, Grant No. PIRSES-2009-GA-246806; and UNESCO.

Last modified on 2018-06-18.